

PAN-STARRS PIXEL ANALYSIS : SOURCE DETECTION AND CHARACTERIZATION

EUGENE A. MAGNIER,¹ W. E. SWEENEY,¹ K. C. CHAMBERS,¹ H. A. FLEWELLING,¹ M. E. HUBER,¹ P. A. PRICE,² C. Z. WATERS,¹ L. DENNEAU,¹ P. DRAPER,³ R. JEDICKE,¹ K. W. HODAPP,¹ N. KAISER,¹ R.-P. KUDRITZKI,¹ N. METCALFE,³ C. W. STUBBS,² R. J. WAINSCOT¹*Draft version January 29, 2019*

ABSTRACT

Over 3 billion astronomical sources have been detected in the more than 22 million orthogonal transfer CCD images obtained as part of the Pan-STARRS1 3π survey. Over 85 billion instances of those sources have been automatically detected and characterized by the Pan-STARRS Image Processing Pipeline photometry software, *psphot*. This fast, automatic, and reliable software was developed for the Pan-STARRS project, but is easily adaptable to images from other telescopes. We describe the analysis of the astronomical sources by *psphot* in general as well as for the specific case of the 3rd processing version used for the first public release of the Pan-STARRS 3π survey data.

Keywords: Surveys:Pan-STARRS 1

1. INTRODUCTION

The 1.8m Pan-STARRS1 telescope is located on the summit of Haleakala on the Hawaiian island of Maui. The wide-field optical design of the telescope (Hodapp et al. 2004) produces a 3.3 degree field of view with low distortion and minimal vignetting even at the edges of the illuminated region. The optics and natural seeing combine to yield good image quality: 75% of the images have full-width half-max values less than (1.51, 1.39, 1.34, 1.27, 1.21) arcseconds for $(g_{P1}, r_{P1}, i_{P1}, z_{P1}, y_{P1})$, with a floor of ~ 0.7 arcseconds.

The Pan-STARRS1 camera (Tonry & Onaka 2009), known as GPC1, consists of a mosaic of 60 back-illuminated CCDs manufactured by Lincoln Laboratory. The CCDs each consist of an 8×8 grid of 590×598 pixel readout regions, yielding an effective 4846×4868 detector. Initial performance assessments are presented in Onaka et al. (2008). Routine observations are conducted remotely from the Advanced Technology Research Center in Kula, the main facility of the University of Hawaii’s Institute for Astronomy (IfA) operations on Maui. The Pan-STARRS1 filters and photometric system have already been described in detail in Tonry et al. (2012).

For nearly 4 years, from 2010 May through 2014 March, this telescope was used to perform a collection of astronomical surveys under the aegis of the Pan-STARRS Science Consortium. The majority of the time (56%) was spent on surveying the $\frac{3}{4}$ of the sky north of -30 Declination with $g_{P1}, r_{P1}, i_{P1}, z_{P1}, y_{P1}$ filters in the so-called 3π Survey. Another $\sim 25\%$ of the time was concentrated on repeated deep observations of 10 specific fields in the Medium-Deep Survey. The rest of the time was used for several other surveys, including a search for potentially hazardous asteroids in our solar system. The details of the telescope, surveys, and resulting science

publications are described by Chambers et al. (2017).

Pan-STARRS produced its first large-scale public data release, Data Release 1 (DR1) on 16 December 2016. DR1 contains the results of the third full reduction of the Pan-STARRS 3π Survey archival data, identified as PV3. Previous reductions (PV0, PV1, PV2; see Magnier et al. 2017) were used internally for pipeline optimization and the development of the initial photometric and astrometric reference catalog (Magnier et al. 2016). The products from these reductions were not publicly released, but have been used to produce a wide range of scientific papers from the Pan-STARRS 1 Science Consortium members (Chambers et al. 2017). DR1 contained only average information resulting from the many individual images obtained by the 3π Survey observations. A second data release, DR2, was made available 28 January 2019. DR2 provides measurements from all of the individual exposures, and include an improved calibration of the PV3 processing of that dataset.

This is the fourth in a series of seven papers describing the Pan-STARRS1 Surveys, the data reduction techniques and the resulting data products. This paper (Paper IV) describes the details of the source detection and photometry, including point-spread-function and extended source model fitting, and the techniques for “forced” photometry measurements. The software describe here was used with a single consistent set of parameters for the complete PV3 analysis, used for both DR1 and DR2.

Chambers et al. (2017, Paper I) provide an overview of the Pan-STARRS System, the design and execution of the Surveys, the resulting image and catalog data products, a discussion of the overall data quality and basic characteristics, and a brief summary of important results.

Magnier et al. (2017, Paper II) describe how the various data processing stages are organized and implemented in the Imaging Processing Pipeline (IPP), including details of the the processing database which is a critical element in the IPP infrastructure.

Waters et al. (2016, Paper III) describe the details of the pixel processing algorithms, including detrending, warping, and adding (to create stacked images) and subtracting (to create difference images) and resulting image

¹ Institute for Astronomy, University of Hawaii, 2680 Woodlawn Drive, Honolulu HI 96822

² Department of Astrophysical Sciences, Princeton University, Princeton, NJ 08544, USA

³ Department of Physics, Durham University, South Road, Durham DH1 3LE, UK

² Harvard-Smithsonian Center for Astrophysics, 60 Garden Street, Cambridge, MA 02138

products and their properties.

Magnier et al. (2016, Paper V) describe the final calibration process, and the resulting photometric and astrometric quality.

Flewelling et al. (2016, Paper VI) describe the details of the resulting catalog data and its organization in the Pan-STARRS database.

Huber et al. (2017, Paper VII) describe the Medium Deep Survey in detail, including the unique issues and data products specific to that survey. The Medium Deep Survey is not part of Data Releases 1 or 2 and will be made available in a future data release.

2. BACKGROUND

The photometric and astrometric precision goals for the Pan-STARRS1 surveys were quite stringent: photometric accuracy of 10 millimagnitudes, relative astrometric accuracy of 10 milliarcseconds and absolute astrometric accuracy of 100 milliarcseconds with respect to the ICRS reference stars.

An additional constraint on the Pan-STARRS analysis system comes from the high data rate. PS1 produces typically ~ 500 exposures per night, corresponding to ~ 750 billion pixels of imaging data. The images range from high galactic latitudes to the Galactic bulge, so large numbers of measurable stars can be expected in much of the data. The combination of the high precision goals of the astrometric and photometric measurements and the high data rate (and a finite computing budget) mean that the process of detecting, classifying, and measuring the astronomical sources in the image data stream in a timely fashion are a significant challenge.

In order to achieve these ambitious goals, the source detection, classification, and measurement process must be both precise and efficient. Not only is it necessary to make a careful measurement of the flux of individual sources, it is also critical to characterize the image point-spread-function, and its variations across the field and from image to image. Since comparisons between images must be reliable, the measurements must be stable for both photometry and astrometry.

A variety of astronomical software packages perform the basic source detection, measurement, and classification tasks needed by the Pan-STARRS IPP. Each of these programs have their own advantages and disadvantages. Below we discuss some of the most widely used of these other packages, highlighting the features of the programs which are particularly desirable, and noting aspects of the programs which are problematic for the IPP.

- DoPhot : analytical fitted model with aperture corrections. pro: well-tested, stable code. con: limited range of models, algorithm converges slowly to a PSF model, limited tests of PSF validity, inflexible code base, fortran (Schechter et al. 1993).
- DAOPhot : Pixel-map PSF model with analytical component. pro: well-tested, high-quality photometry. con: Difficult to use in an automated fashion, does it handle 2D variations well? (Stetson 1987).
- Sextractor : pure aperture measurement with rudimentary source subtraction. pro: fast, widely used, easy to automate. con: poor source separation in

crowded regions, PSF-modeling was only in beta, not widely used at the time (Bertin & Arnouts 1996).

- galfit : detailed galaxy modeling. not a multi-source PSF analysis tool. con: does not provide a PSF model, not easily automated. very detailed results in very slow processing. only a galaxy analysis program (Peng et al. 2002).
- SDSS phot : con: tightly integrated into the SDSS software environment (Lupton et al. 2001).

When the IPP development was starting, the existing photometry packages either did not meet the accuracy requirements or required too much human intervention to be considered for the needs of PS1. In the case of the SDSS Photo tool, the software was judged to be too tightly integrated to the architecture of SDSS to be easily re-integrated into the Pan-STARRS pipeline. A new photometry analysis package was developed using lessons learned from the existing photometry systems. In the process, the source analysis software was written using the data analysis C-code library written for the IPP, **psLib** (Magnier et al. 2017). Components of the photometry code were integrated into the IPP's mid-level astronomy data analysis toolkit called **psModules** (Magnier et al. 2017). The resulting software, '**psphot**', can be used either as a stand-alone C program, or as a set of library functions which may be integrated into other programs

Several variants of **psphot** have been used in the PS1 PV3 analysis. The main variant of **psphot** operates on a single image, or a group of related images representing the data read from a camera in a single exposure. The images are expected to have already been detrended so that pixel values are linearly related to the flux. The gain may be specified by the configuration system, or a variance image may be supplied. A mask may also be supplied to mark good, bad, and suspect pixels. This variant of **psphot** can be called as a stand-alone program, also called **psphot**. In standard IPP operations, this variant is used as a library call within the analysis program **ppImage** during the CHIP analysis stage.

The variant called **psphotStack** accepts a set of images, each representing the same patch of sky in a different filter, nominally the full *grizy* filter set for the analysis of the PS1 PV3 stack images, though where insufficient data were available in a given filter, a subset of these filters was processed as a group. As discussed in detail below, the **psphotStack** analysis includes the capability of measuring forced PSF photometry in some filter images based on the position of sources detected in the other filters. It also include an option to convolve the set of images to a single, common PSF size across the filters for the purpose of fixed aperture photometry.

Another variant of **psphot** used in the PV3 analysis is called **psphotFullForce**. In this variant, a set of image all representing the same pixels are processed together, with the positions of sources to be analyzed loaded from a supplied file. In this variant of the analysis, sources are not discovered – only the supplied sources are considered. PSF models are determined for each exposure and the forced PSF photometry is measured for all sources. A

subset of sources may also be used to measure forced galaxy shape parameters. As described below, a grid of galaxy models are fitted based on the supplied guess model.

3. PSPHOT DESIGN GOALS

psphot has a number of important requirements that it must meet, and a number of design goals which we believe will help to make it usable in a wide range of circumstances. The critical astronomy-driven measurement goals of the Pan-STARRS project, which drive the design of *psphot*, are the photometric accuracy goal (10 millimagntudes) and the astrometric accuracy goal (10 milliarcseconds). For *psphot*, the photometry accuracy goal implies that the measured photometry of stellar sources must be substantially better than this 10 mmag goal since the photometry error per image is combined with an error in the flat-field calibration and an error in measuring the atmospheric effects. We have set a goal for *psphot* of 3mmag photometric consistency for bright stars between pairs of images obtained in photometric conditions at the same pointing, ie to remove sensitivity to flat-field errors. This goal splits the difference between the three main contributors and still allows some leeway. This requirement must be met for well-sampled images and images with only modest undersampling.

The relative astrometric calibration depends on the consistency of the individual measurements. The measurements from *psphot* must be sufficiently representative of the true source position to enable astrometric calibration at the 10mas level. The error in the individual measurements will be folded together with the errors introduced by the optical system, the effects of seeing, and by the available reference catalogs. We have set a goal for *psphot* of 5mas consistency between the true source position and the measured position given reasonable PSF variations under simulations. This level must be reached for images with 250 mas pixels, implying *psphot* must introduce measurement errors less than 1/50th of a pixel. The choice of 32 bit floating point data values for the source centroids places a numerical limit of $1e-7$ on the accuracy of a pixel relative to the size of a chip (since a single data value is used for X or Y). For the 4800^2 GPC chips, this yields a limit of about 0.25 milliarcsecond.

The design goals for *psphot* are chosen to make the program flexible, general, and able to meet the unknown usage cases future projects may require:

- **Flexible PSF model** Different image sources require different ways of representing the PSF. Ideally, both analytical and pixel-based versions should be possible.
- **PSF spatial variation** Most images result in some spatial PSF variations at a certain level. The PSF representation should naturally incorporate 2-D variations.
- **Flexible non-PSF models** *psphot* must be able to represent PSF-like sources as well as non-PSF sources (e.g., galaxies). It must be easy to add new source models as interesting representations of sources are invented.

- **Clean code base** *psphot* should incorporate a high-degree of abstraction and encapsulation so that changes to the code structure can be performed without pulling the code apart and starting from scratch.
- **PSF validity tests** *psphot* should include the ability to choose different types of PSF models for different situations, or to provide the user with methods for assessing the different PSF models.
- **Careful systematic corrections** *psphot* must carefully measure and correct for the photometric and astrometric trends introduced by using analytical PSF models.
- **User Configurable** *psphot* should allow users to change the options easily and to allow different approaches to the analysis.

4. PSPHOT ANALYSIS PROCESS

4.1. Overview

The *psphot* analysis is divided into several major stages, as listed below.

1. **Image Preparation** Load data, characterize the image background, load or construct variance and mask images.
2. **Initial Source Detection** Smooth, find peaks, measure basic properties.
3. **PSF Determination** Select PSF candidates, perform model fits, build PSF model from fits, select best PSF model class.
4. **Bright Source Analysis** Fit sources with PSFs, determine PSF validity, subtract PSF-like sources, fit non-PSF model(s), select best model class, subtract model.
5. **Faint Source Analysis** Detect low-level sources, measure properties (aperture or PSF)
6. **Extended Source Analysis** Detailed measurements relevant to galaxies and/or other extended (non-PSF) sources.
7. **Aperture corrections** Measure the curve-of-growth, spatial aperture variations, and background-error corrections.
8. **Output** Write out sources in selected format, write out difference image, variance image, etc, as selected.

Table 1 lists the types of analyses performed by *psphot*, specifying which of the *psphot* usage cases performs the given analysis. The table also provides a reference to the section of this paper in which the analysis is described. Not all analyses are relevant to all sources in all images. The table identifies those cases where the analyses are applied to only a subset of all sources.

psphot is highly configurable. Users may choose via the configuration system which of the above analyses are performed. This is useful for testing, but also allows for specialized use cases. For example, the PSF model may already be available from external information, in which case the PSF modeling stage can be skipped.

Table 1
psphot measurements performed

Measurement	Camera	Stack	Forced Warp	Diff	Section	Which
Background Subtraction	Y	Y	Y	N ¹	4.3	N/A
Peaks	Y	Y	N	Y	4.4.1	All
Footprints	Y	Y	N	Y	4.4.2	All
Moments	Y	Y	Y	Y	4.4.3	All
PSF Model	Y	Y	Y	N ²	4.5	Uses bright, unsat. stars
Bright Star Profile	Y	Y	N	Y	4.6.1	Saturated Stars
Radial Profiles v1	Y	Y	N	Y	4.6.3	All
Kron Fluxes	Y	Y	Y	Y	4.6.4	All
Source-Size Tests	Y	Y	N	Y	4.6.5	All
Non-Linear PSF Fits	Y	Y	N	N	4.6.6	$S/N > 20$
Unconvolved Galaxy Model	Y	Y	N	N	4.6.8	$S/N > 20$, extended
Unconvolved Streak Model	N	N	N	Y	4.6.8	$S/N > 20$, extended
Linear PSF Fits	Y	Y	Y	Y	4.7	All
Radial Profiles v2	Y	Y	N	Y	4.8.1	Gal. Latitude Cut
Petrosian Fluxes	N	Y	Y	N	4.8.2	Gal. Latitude Cut
Convolved Galaxy Models	N	Y	N	N	4.8.3	Gal. Latitude Cut, mag cut
Fixed Aperture Photometry	N	Y	Y	N	4.8.4	All
Convolved, Fixed Apertures	N	Y	N	N	4.8.4	All
Aperture Corrections	Y	Y	Y	N	4.9	All
Forced PSF Fluxes	N	N	Y	N	5	All
Forced Galaxy Models	N	N	Y	N	5.1	Have Stack Galaxy Models
Lensing Parameters	N	Y	Y	N		All

¹ Background subtraction is performed by `ppSub` before calling `psphot`

² PSF modeling is performed by `ppSub` on the input warps before calling `psphot`

4.2. Informational and Warning Bit Flags

During the *psphot* analysis, there are a wide variety of conditions which are identified by the analysis software. As part of the output data for each detected source, two fields are provided which encode these conditions as bit values in the two 32-bit integers. The following two tables list the individual bit values in these two fields. These informational and warning bits are described in more detail later in this article. Table 2 lists the flags recorded in the output field `FLAGS`. When data from *psphot* is loaded into a DVO database (Magnier et al. 2016), these values are stored in the field `Measure.photFlags` and exposed in the public database (PSPS Flewelling et al. 2016) in the fields `Detection.infoFlag`, `StackObjectThin.XinfoFlag` (where X is one of *grizy*), and `ForcedWarpMeasurement.FinfoFlag`. Table 3 lists the flags recorded in the output field `FLAGS2`. When data from *psphot* is loaded into a DVO database (Magnier et al. 2016), these values are not currently loaded, but they are exposed in PSPS in the fields `Detection.infoFlag2`, `StackObjectThin.XinfoFlag2` (where X is one of *grizy*), and `ForcedWarpMeasurement.FinfoFlag2`.

4.3. Image Preparation

The first step is to prepare the image for detection of the astronomical sources. We need three separate images: the measured flux (signal image), the corresponding variance image, and a mask defining which pixels are valid and which should be ignored. The signal and variance images are represented internally as 32-bit floating point values. The variance and mask images may either be provided by the user, or they may be automatically generated from the input image, based on configuration-

defined values for the image gain, read-noise, saturation, and so forth. For the function-call form of the program, the flux image is provided in the API, and references to the mask and variance are provided in the configuration information. As in the stand-alone C-program, the variance and mask may be constructed automatically by *psphot*.

The mask is represented as a 16-bit integer image in which a value of 0 represents a valid pixel. Each of the 16 bits define different reasons a pixel should be ignored. This allows us to optionally respect or ignore the mask depending on the circumstance. For example, in some cases, we ignore saturated pixels completely while in other circumstances, it may be useful to know the flux value of the saturated pixel. In addition, the mask pixels are used to define the pixels available during a model fit; those which should be ignored for that specific fit are ‘marked’ by setting a special bit (`MARK = 0x8000`). The initial mask, if not supplied by the user or library calls, is constructed by default from the image by applying three rules: 1) Pixels which are above a specified saturation level are marked as saturated. The level is specified by the camera format keyword `CELL.SATURATION`, which may specify a value or define a header keyword which in turn specifies the value in the image header. In the case of PS1 PV3, the header keyword `MAXLIN` specifies the saturation level for each chip (see Waters et al. 2016). 2) Pixels which are below a user-defined value are considered unresponsive and masked as dead. (camera format keyword `CELL.BAD = 0` for PS1 PV3). 3) Pixels which lie outside of a user-defined coordinate window are considered non-data pixels (e.g., overscan) and are marked as invalid. (*psphot* recipe keywords `XMIN`, `XMAX`, `YMIN`, `YMAX`, all set to 0 for PS1 PV3 – invalid pixels were specified for PS1 PV3 with a supplied mask image (see Waters

Table 2
psphot Detection Flag Values #1

Flag Name	Flag Value	Description
PM_SOURCE_MODE_PSFMODEL	0x00000001	Source fitted with a psf model (linear or non-linear)
PM_SOURCE_MODE_EXTMODEL	0x00000002	Source fitted with an extended-source model
PM_SOURCE_MODE_FITTED	0x00000004	Source fitted with non-linear model (PSF or EXT; good or bad)
PM_SOURCE_MODE_FAIL	0x00000008	Fit (non-linear) failed (non-converge, off-edge, run to zero)
PM_SOURCE_MODE_POOR	0x00000010	Fit succeeds, but low-SN, high-Chisq, or large (for PSF – drop?)
PM_SOURCE_MODE_PAIR	0x00000020	Source fitted with a double psf
PM_SOURCE_MODE_PSFSTAR	0x00000040	Source used to define PSF model
PM_SOURCE_MODE_SATSTAR	0x00000080	Source model peak is above saturation
PM_SOURCE_MODE_BLEND	0x00000100	Source is a blend with other sources ¹
PM_SOURCE_MODE_EXTERNAL	0x00000200	Source based on supplied input position
PM_SOURCE_MODE_BADPSF	0x00000400	Failed to get good estimate of object’s PSF
PM_SOURCE_MODE_DEFECT	0x00000800	Source is thought to be a defect
PM_SOURCE_MODE_SATURATED	0x00001000	Source is thought to be saturated pixels (bleed trail)
PM_SOURCE_MODE_CR_LIMIT	0x00002000	Source has crNsigma above limit
PM_SOURCE_MODE_EXT_LIMIT	0x00004000	Source has extNsigma above limit
PM_SOURCE_MODE_MOMENTS_FAILURE	0x00008000	could not measure the moments
PM_SOURCE_MODE_SKY_FAILURE	0x00010000	could not measure the local sky
PM_SOURCE_MODE_SKYVAR_FAILURE	0x00020000	could not measure the local sky variance
PM_SOURCE_MODE_BELOW_MOMENTS_SN	0x00040000	moments not measured due to low S/N. ¹
PM_SOURCE_MODE_BIG_RADIUS	0x00100000	poor moments for small radius, try large radius
PM_SOURCE_MODE_AP_MAGS	0x00200000	source has an aperture magnitude
PM_SOURCE_MODE_BLEND_FIT	0x00400000	source was fitted as a blend
PM_SOURCE_MODE_EXTENDED_FIT	0x00800000	full extended fit was used
PM_SOURCE_MODE_EXTENDED_STATS	0x01000000	extended aperture stats calculated
PM_SOURCE_MODE_LINEAR_FIT	0x02000000	source fitted with the linear fit
PM_SOURCE_MODE_NONLINEAR_FIT	0x04000000	source fitted with the non-linear fit
PM_SOURCE_MODE_RADIAL_FLUX	0x08000000	radial flux measurements calculated
PM_SOURCE_MODE_SIZE_SKIPPED	0x10000000	size could not be determined ¹
PM_SOURCE_MODE_ON_SPIKE	0x20000000	peak lands on diffraction spike
PM_SOURCE_MODE_ON_GHOST	0x40000000	peak lands on ghost or glint
PM_SOURCE_MODE_OFF_CHIP	0x80000000	peak lands off edge of chip

¹ Not used for DR1 or DR2.

et al. 2016).

The library functions used by *psphot* understand two types of masked pixels: “bad” and “suspect”. Bad pixels are those which should not be used in any operations, while suspect pixels are those for which the reported signal may be contaminated or biased, but may be usable in some contexts. For example, a pixel with poor charge transfer efficiency is likely to be too untrustworthy to use in any circumstance, while a pixel in which persistence ghosts have been subtracted might be useful for detection or even analysis of brighter sources. Table 4 lists the 16 bit values used for PS1 mask images, along with their description (see Waters et al. 2016, for additional information).

The variance image, if not supplied, is constructed by default from the flux image using the configuration supplied gain and read noise values to calculate the appropriate Poisson statistics for each pixel. The parameters are determined based on the camera format keywords CELL.GAIN and CELL.READNOISE, which in the case of PS1 PV3 refer to the header keywords GAIN and RDNOISE. In this case, the image is assumed to represent the read-out from a single detector, with well-defined gain and read noise characteristics. This assumption is not always valid. For example, if the input flux image is the result of an image stack with a variable number of input measurements per pixel (due to masking and dithering), the variance cannot be calculated from the signal image

alone. It is necessary in such a case to supply a variance image which accurately represents the variance as a function of position in the image.

Some image processing steps introduce cross-correlation between pixel fluxes. An obvious case is smoothing, but geometric transformations which redistribute fractional flux between neighboring pixels also introduces cross-correlations. In the noise model, it is necessary to track the impact of the cross correlations on the per-pixel variance. In the general case, this would require a complete covariance image, consisting of the set of cross-correlated pixels for each image pixel. Since a typical smoothing or warping operation may introduce correlation between 25 - 100 neighboring pixels, the size of such a covariance image is prohibitive.

Before sources are detected in the image, a model of the background is subtracted. The image is divided into a grid of background points with a spacing defined by the *psphot* recipe values BACKGROUND.XBIN, BACKGROUND.YBIN, set to 400 pixels for PS1 PV3. Superpixels of size BACKGROUND.XSAMPLE, BACKGROUND.YSAMPLE (2×2 for PS1 PV3) times larger than this spacing are used to measure the local background for each background grid point, thus oversampling the background spatial variations. In the interest of speed, a subset of IMSTATS_NPIX (10,000 for PS1 PV3) randomly selected *unmasked* pixels in these regions are used to determine the background. The background

Table 3
psphot Detection Flag Values #2

Flag Name	Flag Value	Description
PM_SOURCE_MODE2_DIFF_WITH_SINGLE	0x00000001	diff source matched to a single positive detection
PM_SOURCE_MODE2_DIFF_WITH_DOUBLE	0x00000002	diff source matched to positive detections in both images
PM_SOURCE_MODE2_MATCHED	0x00000004	source generated based on another image
PM_SOURCE_MODE2_ON_SPIKE	0x00000008	> 25% of (PSF-weighted) pixels land on diffraction spike
PM_SOURCE_MODE2_ON_STARCORE	0x00000010	> 25% of (PSF-weighted) pixels land on starcore
PM_SOURCE_MODE2_ON_BURNTOOL	0x00000020	> 25% of (PSF-weighted) pixels land on burnttool
PM_SOURCE_MODE2_ON_CONVPOOR	0x00000040	> 25% of (PSF-weighted) pixels land on convpoor
PM_SOURCE_MODE2_PASS1_SRC	0x00000080	source detected in first pass analysis
PM_SOURCE_MODE2_HAS_BRIGHTER_NEIGHBOR	0x00000100	peak is not the brightest in its footprint
PM_SOURCE_MODE2_BRIGHT_NEIGHBOR_1	0x00000200	$flux_n / (r^2 flux_p) > 1$
PM_SOURCE_MODE2_BRIGHT_NEIGHBOR_10	0x00000400	$flux_n / (r^2 flux_p) > 10$
PM_SOURCE_MODE2_DIFF_SELF_MATCH	0x00000800	positive detection match is probably this source
PM_SOURCE_MODE2_SATSTAR_PROFILE	0x00001000	saturated source is modeled with a radial profile
PM_SOURCE_MODE2_ECONTOUR_FEW_PTS	0x00002000	too few points to measure the elliptical contour
PM_SOURCE_MODE2_RADBIN_NAN_CENTER	0x00004000	radial bins failed with too many NaN center bin
PM_SOURCE_MODE2_PETRO_NAN_CENTER	0x00008000	petrosian radial bins failed with too many NaN center bin ¹
PM_SOURCE_MODE2_PETRO_NO_PROFILE	0x00010000	petrosian not build because radial bins missing
PM_SOURCE_MODE2_PETRO_INSIG_RATIO	0x00020000	insignificant measurement of petrosian ratio
PM_SOURCE_MODE2_PETRO_RATIO_ZEROBIN	0x00040000	petrosian ratio in the 0th bin (likely bad)
PM_SOURCE_MODE2_EXT_FITS_RUN	0x00080000	we attempted to run extended fits on this source
PM_SOURCE_MODE2_EXT_FITS_FAIL	0x00100000	at least one of the model fits failed
PM_SOURCE_MODE2_EXT_FITS_RETRY	0x00200000	trailed asteroid model fit was re-tried with new window
PM_SOURCE_MODE2_EXT_FITS_NONE	0x00400000	ALL of the model fits failed

¹ Not used for DR1 or DR2.

Table 4
psphot / GPC1 Mask Image Pixel Values

Mask Name	Mask Value	Dynamic?	Suspect?	Description
DETECTOR	0x0001	N	N	A detector defect is present.
FLAT	0x0002	N	N	The flat field model does not calibrate the pixel reliably.
DARK	0x0004	N	N	The dark model does not calibrate the pixel reliably.
BLANK	0x0008	N	N	The pixel does not contain valid data.
CTE	0x0010	N	N	The pixel has poor charge transfer efficiency.
SAT	0x0020	Y	N	The pixel is saturated.
LOW	0x0040	Y	N	The pixel has a lower value than expected.
SUSPECT	0x0080	Y	Y	The pixel is suspected of being bad ¹ .
BURNTOOL	0x0080	Y	Y	The pixel contain an burnttool repaired streak.
CR	0x0100	Y	N	A cosmic ray is present.
SPIKE	0x0200	Y	Y	A diffraction spike is present.
GHOST	0x0400	Y	Y	An optical ghost is present.
STREAK	0x0800	Y	Y	A streak is present.
STARCORE	0x1000	Y	Y	A bright star core is present.
CONV.BAD	0x2000	Y	N	The pixel is bad after convolution with a bad pixel.
CONV.POOR	0x4000	Y	Y	The pixel is poor after convolution with a bad pixel.
MARK	0x8000	X	X	An internal flag for temporarily marking a pixel.

¹ The SUSPECT bit is generic and only used if a specific reason cannot be identified.

It is overloaded on the same bit as BURNTOOL.

value for each superpixel is determined by fitting a Gaussian distribution to the histogram of pixels values.

If the image were empty of stars and only contained flux from a uniform background sky, we would expect the distribution to be Poisson distributed, and in general in a high-enough signal range to be essentially Gaussian. We fit a symmetric Gaussian to all histogram bins within 15% of the peak bin value to determine the mean and standard deviation values for the background.

If, however, the sky is not empty of stars or other

sources, and we have correctly masked the large majority of non-responsive pixels, then we expect the flux distribution of the pixels to be asymmetric with a Gaussian core representing the sky and a tail to the high end representing the pixels with astronomical source flux contributions. We would like to determine the mean of the underlying Gaussian without suffering bias from the stellar flux. We thus perform a second Gaussian fit using an asymmetric subset of the histogram pixels, fitting those histogram bins which are left of the peak but for which

the bin value is greater than 25% of the peak bin, or right of the peak but only using those bins for which the bin value is greater than 50% of the peak bin value.

If the fit to the asymmetric lower fraction of the curve is less than the symmetric fit, but greater than the above lower-bound of the full symmetric fit, then the lower fraction value is kept as the true mean sky value for this superpixel.

Bilinear interpolation is used to generate a full-resolution image from the grid of background points, and this image is then subtracted from the science image. The background image and the background standard deviation image are kept in memory from which the values of `SKY` and `SKY_SIGMA` are calculated for each source in the output catalog. For more details of the background subtraction, see the discussion in Section 2.7 of Waters et al. (2016).

4.4. Initial Source Detection

4.4.1. Peak Detection

The sources are initially detected by finding the location of local peaks in the image. The flux and variance images are smoothed with a small circularly symmetric kernel using a two-pass 1D Gaussian. The smoothed flux and variance images are combined to generate a significance image in signal-to-noise units, including correction for the covariance, if known. At this stage, the goal is only to detect the brighter sources, above a user defined S/N limit (configuration keyword: `PEAKS_NSIGMA_LIMIT` = 20.0 for PS1 PV3). A maximum of `PEAKS_NMAX` (5000 of PS1 PV3) are found at this stage. The detection efficiency for the brighter sources is not strongly dependent on the form of this smoothing function.

The local peaks in the smoothed image are found by first detecting local peaks in each row. For each peak, the neighboring pixels are then examined and the peak is accepted or rejected depending on a set of simple rules. First, any peak which is greater than all 8 neighboring pixels is kept. Any peak which is lower than any of the 8 neighboring pixels is rejected. Any peak which has the same value as any of the other 8 pixels is kept if the pixel X and Y coordinates are greater than or equal to the other equal value pixels. This simple rule set means that a flat-topped region will result peaks at the maximum X and Y corners of the region.

We use the 9 pixels which include the source peak to fit for the position and position errors. We model the peak of the sources as a 2D quadratic polynomial, and use a very simple bi-quadratic fit to these pixels. We use the following function to describe the peak

$$f(x, y) = C_{00} + C_{10}x + C_{01}y + C_{11}xy + C_{20}x^2 + C_{02}y^2$$

and write the Chi-Square equation:

$$\chi^2 = \sum_{i,j} (F_{i,j} - f(x, y))^2 / \sigma_{i,j}^2$$

By approximating the error per pixel as the error on just the peak, and pulling that term out of the above equation, and recognizing that the values x, y in the 3×3 grid centered on the peak pixel have values of only 0 or 1, we can greatly simplify the chi-square equation to a

square matrix equation with the following values:

$$\begin{pmatrix} 9 & 0 & 0 & 0 & 6 & 6 \\ 0 & 6 & 0 & 0 & 0 & 0 \\ 0 & 0 & 6 & 0 & 0 & 0 \\ 0 & 0 & 0 & 6 & 0 & 0 \\ 6 & 0 & 0 & 0 & 6 & 4 \\ 6 & 0 & 0 & 0 & 4 & 6 \end{pmatrix} \begin{pmatrix} C_{00} \\ C_{10} \\ C_{01} \\ C_{11} \\ C_{20} \\ C_{02} \end{pmatrix} = \begin{pmatrix} \sum F_{i,j} \\ \sum F_{i,j}x \\ \sum F_{i,j}y \\ \sum F_{i,j}xy \\ \sum F_{i,j}x^2 \\ \sum F_{i,j}y^2 \end{pmatrix}$$

Inverting the 3×3 matrix terms for C_{00} , C_{20} , and C_{02} , the location of the peak is determined from the minimum of the bi-quadratic function above, and is given by:

$$x_{min} = (C_{11}C_{01} - 2C_{02}C_{10})D^{-1} \quad (1)$$

$$y_{min} = (C_{11}C_{10} - 2C_{20}C_{01})D^{-1} \quad (2)$$

$$D = 4C_{20}C_{02} - C_{11}^2 \quad (3)$$

The resulting peak position, (x_{min}, y_{min}) , is used as the default starting coordinate for the source. Later in the *psphot* analysis, improved measurements of the source positions are calculated as discussed below.

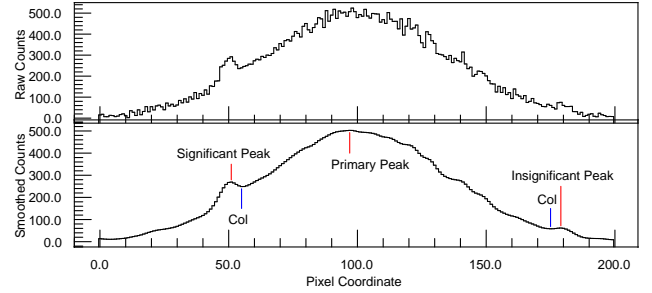


Figure 1. Illustration of peak finding and culling peaks within a footprint. Insignificant peaks within the footprint of a brighter peak are ignored in further processing.

4.4.2. Footprints

The peaks detected in the image may correspond to real sources, but they may also correspond to noise fluctuations, especially in the wings of bright stars. *psphot* attempts to identify peaks which may be formally significant, but are not locally significant. It first generates a set of “footprints”, contiguous collections of pixels in the smoothed significance image above the detection threshold (`PEAKS_NSIGMA_LIMIT`). These regions are grown by a small amount to avoid errors on rough edges – an image of the footprints is convolved with a disk of radius `FOOTPRINT_GROW_RADIUS` (= 3 pixels for PS1 PV3). Peaks are assigned to the footprints in which they are contained (note by construction all peaks must be located in a footprint since the peaks must be above the detection threshold).

For any peak which is not the brightest peak in that footprint it is possible to reach the brightest peak by following the highest valued pixels between the two peaks. The lowest pixel along this path is the *key col* for this peak (as used in topographic descriptions of a mountain). If the key col for a given peak is less than `FOOTPRINT_CULL_NSIGMA_DELTA` (4.0 for PS1 PV3) sigmas below the peak of interest, the peak is considered

to be *locally insignificant* and removed from the list of possible detections (see Figure 1). In the vicinity of a saturated star, the rule is somewhat more aggressive as the flat-topped or structured saturated top of a bright star may appear as multiple peaks with highly significant cols between them. However, this is an artifact of the proximity to saturation. Sources for which the peak is greater than 50% of the saturation value require the col to also be a fixed fraction (5%) of the saturation below the peak to avoid being marked as locally insignificant.

Sometimes it is useful to know if a source has a near neighbor which may be affecting the photometry. Three flag bits are used to identify such possible situations. Peaks which are *not* the brightest peak within a single footprint have the flag bit `PM_SOURCE_MODE2_HAS_BRIGHTER_NEIGHBOR` set. This is a fairly common situation. We also define the following ratio to compare the flux of the bright source to the flux of a neighbor scaled by intervening area: $R = \frac{f_n}{r^2 f_p}$ where f_n is the flux of the brightest neighbor in the footprint, f_p is the flux of the source of interest, and r is the separation between the two sources. If $R > 1$, the flag bit `PM_SOURCE_MODE2_HAS_BRIGHT_NEIGHBOR_1` is set. If $R > 10$, the flag bit `PM_SOURCE_MODE2_HAS_BRIGHT_NEIGHBOR_10` is set.

4.4.3. Centroid and Higher-Order Moments

Once a collection of peaks has been identified, a number of basic properties of the sources related to the first, second, and higher moments are measured. Below, the second moments are used to select candidate stellar sources to be used in modeling the PSF.

In order to measure the moments, it is necessary to define an appropriate aperture in which the moments are measured. We also apply a “window function”, down-weighting the pixels by a Gaussian, centered on the object, with size σ_w chosen to be large compared to the PSF size, σ_{PSF} . This window function reduces the noise of the measurement of the moments by suppressing the noisy pixels at high radial distance as well as by reducing the contaminating effects of neighboring stars. The choice of σ_w and the aperture is an iterative process: for a given value of σ_w , the PSF stars will have a measured value of the PSF size, σ'_{PSF} which different from the true value due to the effect of the window function. The measured value of the PSF size will be biased high or low depending on both the signal-to-noise of the source and the size of the window function compared to the true PSF size.

These effects are illustrated in Figure 2 using simulated data. An image was generated with a PSF model matching the radial profile of the PS1 PSF model with σ_{PSF} corresponding to a FWHM of 1.4 arcseconds. As the window function σ_w is increased, the measured FWHM for the bright simulated stars rises to meet the truth value. For small values of σ_w , fainter stars are biased to low measured values of the FWHM. For large values of σ_w , the faint stars are biased to higher values and the scatter increases. We attempt to minimize the scatter and trends with magnitude at the cost of overall bias.

In a real image, we do not know the true value of the PSF size. If we simply choose a very large window function and rely on bright stars, our estimate of the PSF size

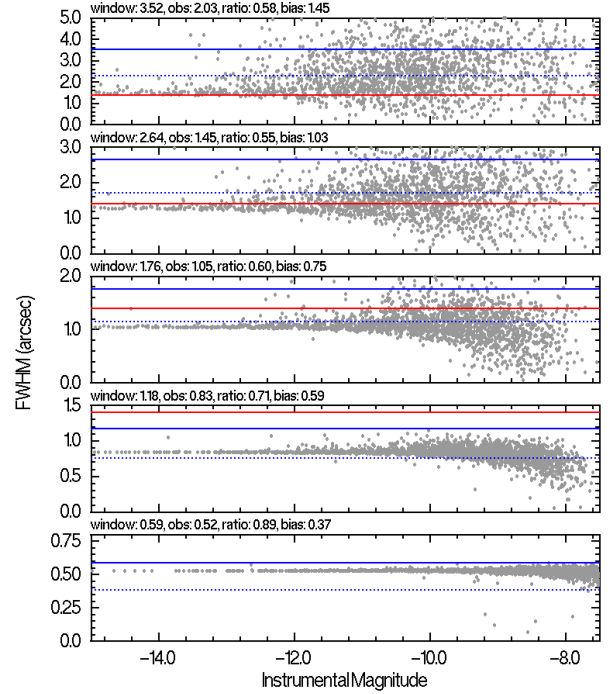


Figure 2. Example of the biases encountered when measuring the second moments. A simulated image was generated using the PS1 PSF profile. Each panel corresponds to a different value of σ_w , corresponding to the window FWHM values as marked. The solid red line is the true FWHM of the PSF used to generate the stars (1.4 arcsec in all cases). The blue solid line is the FWHM of the window function. The gray dots are the FWHM derived from the measured second moments for stars in the image. The median of this distribution (mag < -10) is listed as “obs”. The ratio of the median FWHM to the FWHM of the window function is listed as “ratio”, while the ratio of the median FWHM to the true stellar FWHM is listed as “bias”. The dotted blue line is the target (65% of the window function). In this example, we would choose σ_w between 0.5 and 0.8 arcseconds so the dotted blue line would match the bright end of the gray dots. See discussion in the text for the choice of target window.

will be quite noisy. Compounding this problem are the two additional facts that (1) we do not know which are the real stars (as opposed to bright galaxies or possible image artifacts) and (2) the brighter stars are themselves subject to additional biases due to saturation and other non-linear effects (c.f., “the Brighter-Fatter” effect, Antilogus et al. 2014; Gruen et al. 2015). To make a robust choice for σ_w , we choose a value such that the measured value of σ'_{PSF} is 65% of σ_w . The resulting second moment values are biased somewhat low ($\sim 75\%$ of the truth value for the PS1 PSF profile), but are relatively unbiased as a function of brightness.

To choose the value of σ_w , we try a sequence of values spanning a range guaranteed to contain any reasonable seeing values. The values are specified in the *psphot* recipe as `PSF.SIGMA.VALUES` and have the following values for PS1 PV3: (1, 2, 3, 4.5, 6, 9, 12, 18) pixels \sim (0.26, 0.51, 0.77, 1.15, 1.54, 2.3, 3.1, 4.6) arcseconds. For each of these σ_w values, we then select candidate PSF stars based on the distribution of the measured σ'_{PSF} in the two principal directions: $\sigma_{x,x}$ and $\sigma_{y,y}$ (see Section 4.5.2, below). For each test value of σ_w , we determine the ratio $\rho\sigma = \frac{\sigma_x + \sigma_y}{2\sigma_w}$, i.e., the ratio of the window size to the observed PSF size. We interpolate to find a value of σ_w for

which ρ_σ is expected to be 0.65. We use an aperture with a radius of $4\sigma_w$ to select the pixels for the measurement of the moments.

Once σ_w has been determined, moments are measured as defined below.

$$x_0 = \frac{1}{S} \sum_i w_i (f_i - s_i) x_i \quad (4)$$

$$y_0 = \frac{1}{S} \sum_i w_i (f_i - s_i) y_i \quad (5)$$

$$M_{xx} = \frac{1}{S} \sum_i w_i (f_i - s_i) (x_i - x_0)^2 \quad (6)$$

$$M_{xy} = \frac{1}{S} \sum_i w_i (f_i - s_i) (x_i - x_0) (y_i - y_0) \quad (7)$$

$$M_{yy} = \frac{1}{S} \sum_i w_i (f_i - s_i) (y_i - y_0)^2 \quad (8)$$

$$M_{xxx} = \frac{1}{S} \sum_i \frac{w_i}{r_i} (f_i - s_i) (x_i - x_0)^3 \quad (9)$$

$$M_{xxy} = \frac{1}{S} \sum_i \frac{w_i}{r_i} (f_i - s_i) (x_i - x_0)^2 (y_i - y_0) \quad (10)$$

$$M_{xyy} = \frac{1}{S} \sum_i \frac{w_i}{r_i} (f_i - s_i) (x_i - x_0) (y_i - y_0)^2 \quad (11)$$

$$M_{yyy} = \frac{1}{S} \sum_i \frac{w_i}{r_i} (f_i - s_i) (y_i - y_0)^3 \quad (12)$$

$$M_{xxxx} = \frac{1}{S} \sum_i \frac{w_i}{r_i^2} (f_i - s_i) (x_i - x_0)^4 \quad (13)$$

$$M_{xxxxy} = \frac{1}{S} \sum_i \frac{w_i}{r_i^2} (f_i - s_i) (x_i - x_0)^3 (y_i - y_0) \quad (14)$$

$$M_{xxxyy} = \frac{1}{S} \sum_i \frac{w_i}{r_i^2} (f_i - s_i) (x_i - x_0)^2 (y_i - y_0)^2 \quad (15)$$

$$M_{xyyyy} = \frac{1}{S} \sum_i \frac{w_i}{r_i^2} (f_i - s_i) (x_i - x_0) (y_i - y_0)^3 \quad (16)$$

$$M_{yyyyy} = \frac{1}{S} \sum_i \frac{w_i}{r_i^2} (f_i - s_i) (y_i - y_0)^4 \quad (17)$$

where f_i is the flux in a pixel; s_i is the local sky value for that pixel; w_i is the value of the window function for the pixel; $S = \sum_i (f_i - s_i) w_i$ is the window-weighted sum of the source flux, used to re-normalize the moments; r_i is the radius of a pixel, $\sqrt{(x_i - x_0)^2 + (y_i - y_0)^2}$; The sums are performed over all (unmasked) pixels in the aperture. For the centroid calculation (x_0, y_0) , the peak coordinate (see 4.4.1) is used to define the aperture and the window function; for higher order moments, the centroid is used to center the window function.

For sources with peak flux above the saturation limit, the moments are generally poorly measured if the aperture defined by σ_w is used. For these sources, the quality of the measurement is compromised by the saturation. However, it is still useful to estimate the first and second moments of the source in order to allow a crude measurement of the brightness from the wings of the source. In

this case, a larger aperture, 3 times the standard aperture, is used to make a crude estimate. For such sources, the flag bit `PM_SOURCE_MODE_BIG_RADIUS` is set and the source is ignored in all analyses below except for the analysis applied to very bright stars (Section 4.6.1).

If the measured centroid coordinates (x_0, y_0) differ from the peak coordinates by a large amount ($1.5\sigma_w$), then the peak is identified as being of poor quality and is skipped in further analyses; the flag bit `PM_SOURCE_MOMENTS_FAILURE` is set for such sources. In such a case, it is likely that the ‘peak’ was identified in a region of flat flux distribution or many saturated or edge pixels. During the analysis of the moments, the background (“sky”) model is also examined for the location of each source. The value of the background and the variance of the background are recorded for each source. In some cases, the sky model or the variance is not well defined at the location of a specific sources (e.g., due to an extrapolation failure). In these cases, the flag bits `PM_SOURCE_SKY_FAILURE` or `PM_SOURCE_SKYVAR_FAILURE` are set as appropriate and the measurement of the moments is skipped.

In addition to the moments above, the 1st and half-radial moments, M_r and M_h as defined below, are calculated:

$$M_r = \frac{1}{S} \sum_i (f_i - s_i) r_i \quad (18)$$

$$M_h = \frac{1}{S} \sum_i (f_i - s_i) \sqrt{r_i} \quad (19)$$

Note that the window function is not applied in the calculation of these moments.

With the first radial moment, we can calculate a preliminary Kron radius and magnitude. The Kron radius (Kron 1980) is defined to be $2.5\times$ the first radial moment. The Kron flux is the sum of (sky-subtracted) pixel fluxes within the Kron radius. We also calculate the flux in two related annular apertures: the Kron inner flux is the sum of pixel values for the annulus $R_1 < r < 2.5R_1$, while the Kron outer flux is the sum of pixel values for $2.5R_1 < r < 4R_1$. The first radial moment is limited at the low and high ends by $R_{\min} < M_r < R_{\max}$ where R_{\min} is the first radial moment of the PSF stars, or $0.75\sigma_w$ if that cannot be determined. R_{\max} is set to the size of the moments aperture, $4\sigma_w$. These Kron measurements are performed for all sources with a valid set of moments. At this stage, the measurement of the Kron parameters are preliminary since the aperture has been chosen as a fixed size relative to the size of the PSF. At a later stage, higher-quality Kron parameters appropriate to galaxies are measured with more care paid to the exact aperture used (Section 4.6.4).

4.5. PSF Determination

4.5.1. PSF Model vs Source Model

The point-spread-function (PSF) of an image describes the shape of all unresolved sources in the image. In a typical wide-field image, the shape of unresolved sources varies as a function of position in the image. The full PSF thus needs to include a model with parameters which vary across the image.

The PSF used by *psphot* consists of an analytical

function combined with a pixelized representation of the residual differences between the analytical model and the true PSF. Both the shape parameters of the analytical model and the pixelized residual differences are allowed to vary in two dimensions across the images.

Within *psphot*, several analytical models may be used to describe the smooth portion of the PSF, but all share a few common characteristics. As an example, a simple model consists of a 2-D elliptical Gaussian:

$$f(x, y) = I_o e^{-z} + S \quad (20)$$

$$z = \frac{x^2}{2\sigma_x^2} + \frac{y^2}{2\sigma_y^2} + \sigma_{xy}xy \quad (21)$$

$$x = x_{\text{ccd}} - x_o \quad (22)$$

$$y = y_{\text{ccd}} - y_o \quad (23)$$

Here the model parameters consist of the centroid coordinates (x_o, y_o) , the elliptical shape parameters $(\sigma_x, \sigma_y, \sigma_{xy})$, the model normalization (I_o) and the local value of the background (S) .

A specific source will have a particular set of values for the model parameters, some of which depend on the PSF model and the position of the source in the image, while the rest are unique to the individual source. For the case of the elliptical Gaussian model, the PSF parameters would be the shape terms $(\sigma_x, \sigma_y, \sigma_{xy})$ while the independent parameters would be the centroid, normalization and local sky values (x_o, y_o, I_o, S) . Thus the shape parameters are each a function of the source centroid coordinates:

$$\sigma_x = f_1(x_{\text{ccd}}, y_{\text{ccd}}) \quad (24)$$

$$\sigma_y = f_2(x_{\text{ccd}}, y_{\text{ccd}}) \quad (25)$$

$$\sigma_{xy} = f_3(x_{\text{ccd}}, y_{\text{ccd}}). \quad (26)$$

psphot represents the variation in the PSF parameters as a function of position in the image in two possible ways, specified by the configuration. The first option is to use a 2-D polynomial which is fitted to the measured parameter values across the image. The second option is to use a grid of values which are measured for sources within a subregion of the image. In the latter case, the value at a specific coordinate in the image is determined by interpolation between the nearest grid points. The order of the polynomial or the sampling size of the grid is dynamically determined depending on the number of available PSF stars. In the case of the PV3 analysis, the grid of values was used, with a maximum of 6×6 samples per GPC1 chip image. For the earlier PV2 analysis, the maximum grid sampling was 3×3 per GPC1 chip image. For the PV1 analysis, the polynomial representation was used, with up to 3rd order terms. The higher order representation was used for PV3 in order to follow some of the observed PSF variations in the images.

Several analytical functions which are likely candidates to describe the smooth portion of the PSF are available in *psphot*:

- Gaussian : $f = I_o e^{-z}$
- Pseudo-Gaussian : $f = I_o(1 + z + \frac{1}{2}z^2 + \frac{1}{6}z^3)^{-1}$ [PGAUSS]
- Variable Power-Law : $f = I_o(1 + z + z^\alpha)^{-1}$ [RGAUSS]

- Steep Power-Law : $f = I_o(1 + \kappa z + z^{2.25})^{-1}$ [QGAUSS]
- PS1 Power-Law : $f = I_o(1 + \kappa z + z^{1.67})^{-1}$ [PS1_V1]

The Pseudo-Gaussian is a Taylor expansion of the Gaussian and is used by Dophot (Schechter et al. 1993). The latter profiles are similar to the Moffat profile form (Moffat 1969; Buonanno et al. 1983), with small differences. A user may choose to try more than one analytical function for a given image. As discussed below (Section 4.5.3), *psphot* can automatically choose the best model based on the quality of the PSF fits.

For the PS1 GPC1 analysis, we used the PS1_V1 model, which we found by experimentation to match well to the observed profiles generated by PS1. Figure 3 shows example radial profiles for moderately bright stars in fairly good (0.9 arcsec) and poor (2.2 arcsec) seeing. Using a fixed power-law exponent results in somewhat faster profile fitting compared to the variable power-law exponent model.

The analytical models in *psphot* are written with a high degree of code abstraction making it relatively easy to add different analytical models to the software. The same portion of code used to describe the analytical portion of the PSF sources is also used to for galaxy models.

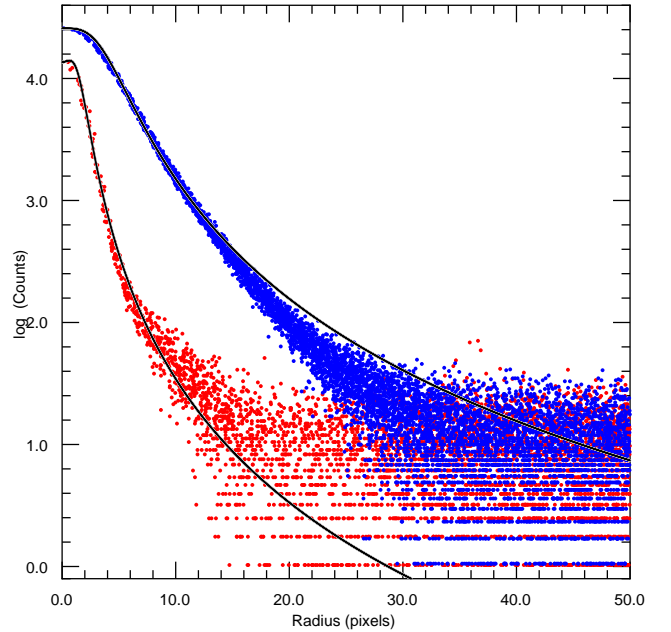


Figure 3. Radial profiles of stellar images from PS1. These two profiles illustrate the radial trend of the PS1 PSFs for a star with FWHM 0.9 arcsec (red) and 2.2 arcsec (blue). The black line shows the PSF model with radial trend of the form $(1 + \kappa r^2 + r^{3.33})^{-1}$.

Once the smooth component of the PSF has been fitted with an analytical model, a pixel representation of the residuals is generated. This representation is constructed as an image of the expected residuals for any position in the image. The value of each pixel in the image model is determined from 2D fits to the measured residuals of the PSF stars.

The residual model is calculated using the residuals for all PSF stars. The residuals (and their errors) for each

star are renormalized by the flux of the star to put them on a consistent flux scale. For each PSF star, all pixels within a user-specified radius (`PSF.RESIDUALS.RADIUS` = 9) are selected for the measurement. For a given pixel in the model, the pixel values from the PSF stars are interpolated to the center of the model pixel. Pixels may be used in this analysis if their signal-to-noise exceeds a user-defined limit. For the PV3 3π analysis, we allowed all pixels within the user-specified radius, not limiting on the basis of the signal-to-noise.

Pixels for a given star which are more than a number of sigmas (`PSF.RESIDUALS.NSIGMA` = 3.0) deviant from the median value of the pixels from all stars are rejected.

If no spatial variation is allowed, the mean or median value is calculated for the model pixel based on the user-specified mean statistic (`PSF.RESIDUALS.STATISTIC` = `ROBUST_MEDIAN`).

If spatial variation is requested, then the pixel values are fitted to a linear model:

$$\begin{aligned} R[(x_{\text{mod}}, y_{\text{mod}})][(x_{\text{ccd}}, y_{\text{ccd}})] &= R_o[(x_{\text{mod}}, y_{\text{mod}})] \\ &+ R_x[(x_{\text{mod}}, y_{\text{mod}})]x_{\text{ccd}} \\ &+ R_y[(x_{\text{mod}}, y_{\text{mod}})]y_{\text{ccd}} \end{aligned}$$

where $R[(x_{\text{mod}}, y_{\text{mod}})][(x_{\text{ccd}}, y_{\text{ccd}})]$ is the value for model pixel $(x_{\text{mod}}, y_{\text{mod}})$ for a star with centroid at image pixel $(x_{\text{ccd}}, y_{\text{ccd}})$. The parameters R_o , R_x , R_y are determined for each pixel in the model $[(x_{\text{mod}}, y_{\text{mod}})]$.

4.5.2. Candidate PSF Source Selection

The first stage of determining the PSF model for an image is to identify a collection of sources in the image which are *likely* to be unresolved (i.e., stars). *psphot* uses the source sizes as estimated from the second moments to make the initial guess at a collection of unresolved sources. At this point, the program has measured the second order moments for all sources identified by their peaks, as well as an approximate signal-to-noise ratio, above the bright threshold. All sources with a S/N ratio greater than a user-defined parameter (`PSF_SN_LIM` = 20.0 for PS1 PV3) are selected by *psphot*, though sources which have more than a certain number of saturated pixels are excluded at this stage. The program then examines the 2-D plane of $M_{x,x}$, $M_{y,y}$ in search of a concentrated clump of sources (see Figure 4). To do this, it constructs an artificial image with pixels representing the value of $M_{x,x}$, $M_{y,y}$, using $0.1\sigma_w^2$ as the size of a pixel in this artificial image. The binned $M_{x,x}$, $M_{y,y}$ plane is then examined to find a significant peak. Unless the image is extremely sparse, such a peak will be well-defined and should represent the sources which are all very similar in shape. Other sources in the image will tend to land in very different locations, failing to produce a single peak. To avoid detecting a peak from the unresolved cosmic rays, sources which have second-moments very close to 0 are ignored. For these sources, the flag bit `PM_SOURCE_MODE_DEFECT` is set.

Once a peak has been detected in this plane, the centroid and second moments of this peak are measured. All sources which land within 2 pixels of this centroid are selected as candidate PSF sources in the image.

When the second moments are measured, *psphot* also counts the number of saturated pixels within the analysis aperture. If more than a single saturated pixel is found,

and if the second moments of that object are more than one standard deviation larger than the clump identified above, this source is identified as a highly saturated star and marked with the flag bit `PM_SOURCE_MODE_SATSTAR`. Sources which have more than a single saturated pixel, but for which the second moments do not exceed the above limits are marked as likely saturated regions (e.g., bleed trails). These sources are skipping in most additional analyses and are marked with the flag bit `PM_SOURCE_MODE_SATURATED`.

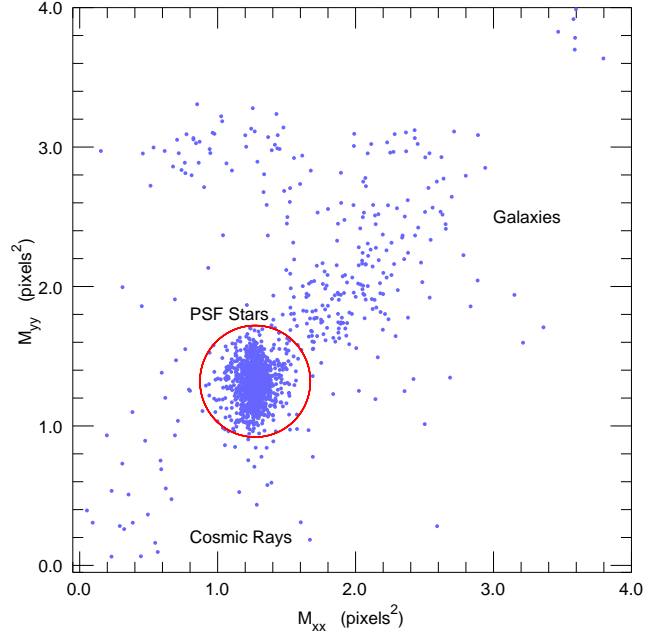


Figure 4. Illustration of PSF star selection using the second moments in X_{ccd} and Y_{ccd} directions. The dominant clump is located in this diagram. Galaxies tend to have a range of sizes and thus spread out above the stars. Cosmic rays also have a range of sizes, with one dimension smaller than the PSF. The red circle represents the PSF star candidates.

4.5.3. Candidate PSF Source Model Fits

All candidate PSF sources are then fitted with the selected source model, allowing all of the parameters (PSF and independent) to vary in the fit. The software uses the Levenberg-Marquardt minimization technique (Press et al. 1992; Madsen et al. 2004) for the non-linear fitting. Non-linear fitting can be very computationally intensive, particularly if the starting parameters are far from the minimization values. The first and second moments are used to make a good guess for the centroid and shape parameters for the PSF models. Any sources which fail to converge in the fit are flagged as invalid.

For the resulting collection of source model parameters, the PSF-dependent parameters of the models are all fitted as a function of position using either the 2-D polynomial or the gridded superpixel representation. The maximum order of these fits depends on the number of PSF sources (see Table 5). The fitting process for these polynomials is iterative, and rejects the 3σ outliers in each of three passes. This fitting technique results in a robust measurement of the variation of the

Table 5

Minimum number of stars required for a given order of the PSF 2D variations.

Minimum Number of Stars	Order	Number of Grid Cells
16	1	4
54	2	9
128	3	16
300	4	25
576	5	36

PSF model parameters as a function of position without being excessively biased by individual sources which are not well described by the PSF model (e.g., galaxies which snuck into the sample). Sources whose model parameters are rejected by this iterative fitting technique are also marked as invalid PSF sources and ignored in the later PSF model fitting stages. Sources which are actually used to define the PSF model for a given image have the flag bit `PM_SOURCE_MODE_PSFSTAR` set.

The order of the fit or number of grid samples is modified if the number of stars available for the fit is insufficient to justify the highest value. Regardless of the requested order, if the number of stars is below the following limits, the order is limited as shown in Table 5. Note that the number of grid cells in one dimension is one greater than the equivalent polynomial order.

All of the PSF-candidate sources are then re-fitted using the PSF model to specify the PSF-dependent model parameter values for each source. For example, in the case of the elliptical Gaussian model, the shape parameters ($\sigma_x, \sigma_y, \sigma_{xy}$) for each source are set by the coordinates of the source centroid and fixed (not allowed to vary) in the fitting procedure. The resulting fitted models are then used to determine a metric which tests the quality of the PSF model for this particular image.

The metric used by *psphot* to assess the PSF model is the scatter in the differences between the aperture and fit magnitudes for the PSF sources. This difference is a critical parameter for any PSF modeling software as it is a measurement of how well the PSF model captures the flux of the star. Aperture photometry is measured for a circular aperture with a radius of `PSF_APERTURE_SCALE` (= 4.5 for the PV3 3π analysis) times σ_w (Section 4.4.3). The average aperture correction ($m_{AP} - m_{PSF}$) is measured and, if multiple PSF model types are selected, the PSF model with the minimum clipped scatter in this statistic is chosen for the image. An approximate aperture correction is measured here, with a more detailed correction measured after all source analysis is performed (see Section 4.9). Sources for which the aperture magnitude is measured have the flag bit `PM_SOURCE_MODE_AP_MAGS` set. These aperture magnitudes are stored in the DVO field `Measure.Map` and exported to the PSPS as a flux in Janskies in the field `Detection.apFlux`. The radius (in arcseconds) of the aperture used for each exposure is reported in PSPS as `Detection.apRadius`, while the unmasked fraction of the aperture is reported in PSPS as `Detection.apFillF`.

When the PSF and aperture photometry for a source is measured, two additional quantities are measured which are useful to assess the quality of the measurements.

First, the mask image is examined and the number of unmasked pixels is summed, weighted by the normalized PSF model. The resulting quantity, `PSF_QF` has a value between 0.0 (totally masked) and 1.0 (totally unmasked). Elsewhere in the IPP system, we use this value to filter out detections which are unreliable due to the masking. For a generous cut, leaning toward completeness at the cost of some lower quality measurements, `PSF_QF` > 0.85 is used in some contexts; in other cases, we require `PSF_QF` > 0.95 to ensure a high-quality measurement (see for example the calculation of average photometry in Magnier et al. 2016). The second quantity is related to the first: `PSF_QF_PERFECT` uses all mask values to assess the quality factor, while `PSF_QF` uses only the “bad” mask bit values (see Section 4.3).

Several flag bits are raised based on statistics which are similar to the `PSF_QF` measurement. First, *psphot* calculates the normalized, PSF-weighted fraction of pixels which are masked due to one of the following four causes: a diffraction spike (`SPIKE`), the core of a saturated star (`CORE`), burntout-subtracted region (`BURNTOUT`), or a pixel for which, due to interpolation or convolution, a significant fraction of the pixel flux comes from a masked pixel. These masking conditions are all treated as “suspect” by *psphot*, which means they are *included* in the analysis of the source pixels. However, since they may potentially affect the photometry (or astrometry), it is useful to note of a source has a non-trivial fraction of these poor mask pixels. If the normalized PSF-weighted fraction of pixels masked due to any of these four conditions exceeds 25%, then one of the following bits is raised for the corresponding condition: `PM_SOURCE_MODE2_ON_SPIKE`, `PM_SOURCE_MODE2_ON_STARCORE`, `PM_SOURCE_MODE2_ON_BURNTOUT`, `PM_SOURCE_MODE2_ON_CONVPOOR`. In addition, the following flag bits may also be raised if the central pixel of a source lands on a pixel masked for a diffraction spike (`PM_SOURCE_MODE_ON_SPIKE`), an optical ghost (`PM_SOURCE_MODE_ON_GHOST`), or off the active pixels of the CCD (`PM_SOURCE_MODE_OFF_CHIP`).

4.6. Bright Source Analysis

Once a PSF model has been determined, the brighter sources in the image may be analyzed in detail. The goals in this stage are (1) to determine the fluxes and positions of the bright stellar sources with high precision appropriate to their high signal-to-noise and (2) to characterize the bright source flux profiles sufficiently well that they may be subtracted from the image to allow for the clean detection of the fainter sources. Note that as the analysis proceeds, there are several stages in which the 2D flux models for all sources are subtracted from the image, and individual sources are replaced in the image for a particular analysis step and then removed again. The flux limit for this analysis stage is user-defined as a signal-to-noise value. In the PV3 analysis of the 3π survey data, this limit was set to a signal-to-noise ratio of 20.0.

In order to allow for multiple threads to process a single image, the pixels in an image are divided into a grid of superpixels. The superpixels are assigned to one of four groups so that each superpixel in a group is well separated from the other superpixels of that group. The

analysis of the image proceeds in 4 steps, one for each of these groups. Each of the superpixels in the first group is assigned to a single thread until all threads are assigned. A single thread is responsible for the analysis of sources which land within their current superpixel, as determined by the centroid coordinates. Since the superpixels in a given thread group are not contiguous by construction, sources near the edge of a superpixel can be analysed by considering the nearby pixels from neighboring superpixel (guaranteed not to be in the current thread group).

As the threads complete their analysis, they are assigned the next unfinished superpixel in the active group. When all superpixels in one group have been processed, then the superpixels in the next group can start. This strategy allows the threading to process sources which may be extended without the danger that two threads are actively touching the same pixels. For the PV3 analysis, 4 threads were used for most processing tasks.

4.6.1. Very Bright Stars

The standard *psphot* PSF modeling code fails to fit the wings of highly saturated stars, especially if the core of the star is too contaminated by saturated pixels. For stars with more than a single saturated pixel, we model the radial profile of the logarithmic instrumental flux in logarithmically spaced radial bins. For each radial bin, we determine the median of the log-flux. This median profile is then interpolated to generate the full radial flux distribution. Note that in the case of very saturated stars, pixels in the central regions are largely masked, because they are saturated. Thus in these cases, the psf-weighted masked fraction (see Section 4.5.3) is generally quite low or 0.0. Sources for which this radial profile is subtracted have the flag bit `PM_SOURCE_MODE2_SATSTAR_PROFILE` set.

4.6.2. Fast Ensemble PSF Fitting

Before the detailed analysis of the sources is performed, it is convenient to subtract off all of the sources, at least as well as possible at this stage. We make the assumption that all sources are PSF-like. If the centroid of the source has been determined, we use this value for its position; otherwise, we use the interpolated position of the peak. A single linear fit is used to simultaneously measure all source fluxes. Since the local sky has been subtracted, this measurement assumes the local sky is zero. We can write a single χ^2 equation for this image:

$$\chi^2 = \sum_{\text{pixels}} (F_{x,y} - \sum_{\text{sources}} A_i P[x_0, y_0])^2$$

where $F_{x,y}$ is image flux for each pixel, $P[x_0, y_0]$ is the PSF model realized at the position of source i , and A_i is the normalization for the source.

Minimizing this equation with respect to each of the A_i values results in a matrix equation:

$$M_{i,j} \bar{A}_i = \bar{F}_j$$

where \bar{A}_i is the vector of A_i values, the elements of $M_{i,j}$ consist of the dot products of the unit-flux PSF for source i and source j , and \bar{F}_j is the dot product of the unit-flux PSF for source j with the pixels corresponding to

source j . The dot products are calculated only using pixels within the source apertures. Since most sources have no overlap with most other sources, this matrix equation results in a very sparse, mostly diagonal square matrix. The dimension is the number of sources, likely to be 1000s or 10,000s. Direct inversion of the matrix would be computationally very slow. However, an iterative solution quickly yields a result with sufficient accuracy. In the iterative solution, a guess at the solution \bar{A} is made assuming $M_{i,j}$ is purely diagonal; the guess is multiplied by $M_{i,j}$, and the result compared with the observed vector \bar{F}_j . The difference is used to modify the initial guess. This process is repeated several times to achieve convergence. Convergence is quick (a few iterations) because of the highly diagonal matrix with small off-diagonal terms: the dot product of source i and source j is 1 where $i = j$ and much less than 1 where $i \neq j$.

Once a solution set for A_i is found, all of the sources are subtracted from the image by applying these values to the unit-flux PSF. Sources for which a PSF model has been fitted (whether or not this is retained as the best model in the end) has the flag field `PM_SOURCE_MODE_PSFMODEL` set. All sources which are included in the ensemble linear fit have the flag bit `PM_SOURCE_MODE_LINEAR_FIT` set, including those for which the model is not the PSF.

4.6.3. Radial Profile Wings

We attempt to measure the radial profile of sources in order to find the radius at which the flux of the source is matches the sky. In this analysis, a series of up to 25 radial bins with power-law spacing are defined and the flux of the source in each annulus is measured. The “sky radius” is defined to be the radius at which the (robust median) flux in the annulus is within 1σ of the local sky level. If this limit is not reached before the slope of the flux from one annulus to the next is less than a user-defined limit, then the annulus at which the slope reaches this limit is used to define the sky radius. These values are saved in the output `smf / cmf` files, but not sent to the PSPS. The sky radius value is used below in the calculation of the Kron magnitude.

4.6.4. Kron Magnitudes

Preliminary Kron radius and flux values (Kron 1980) are calculated soon after sources are detected (Section 4.4.3). However, these preliminary values are not accurate due to the window-functions applied. After sources have been characterized and the PSF model is well-determined, the Kron parameters are re-calculated more carefully. In this version of the calculation, following the algorithm described by Bertin & Arnouts (1996), the image is first smoothed by Gaussian kernel with $\sigma = 1.7$ pixels, corresponding to a FWHM of $1.0''$ in the PS1 stack images. Next, the Kron radius is determined in an iterative process: the first radial moment is measured using the pixels in an aperture $6\times$ the first radial moment from the previous iteration. On the first iteration, the sky radius is used in place of the first radial moment. By default, 2 iterations are performed. The Kron radius is defined to be $2.5\times$ the first radial moment. The Kron flux is the sum of pixel fluxes within the Kron radius. We also calculate the flux in two related annular apertures: the Kron inner flux is the sum of pixel values for

the annulus $R_1 < r < 2.5R_1$, while the Kron outer flux is the sum of pixel values for $2.5R_1 < r < 4R_1$.

Two details in the calculation above should be noted. First, for faint sources, noise in the measurement of the 1st radial moment may result in an excessively small aperture for the successive calculations. The window used for the calculations is constrained to be at least the size of the aperture based on the PSF stars (Section 4.4.3). At the other extreme, noise may make the radius grow excessively, resulting in an unrealistically low effective surface brightness. The aperture is constrained to be less than a maximum value defined such that the minimum surface brightness is $1/2$ times the effective surface brightness of a point source detected at the 5σ limit.

Second, the measurement of the 1st radial moment includes a filter to reduce contamination from outlier pixels. Pairs of pixels on opposite sides of the central pixel are considered together. The geometric mean of the two fluxes is used to replace the flux values. If the source has 180° symmetry, this operation has no impact. However, if one of the two pixels is unusually high, the value will be suppressed by the matched pixel on the other side. This trick has the effect of reducing the impact of pixels which include flux from near neighbors.

4.6.5. Source Size Assessment

After the PSF model has been fitted to all sources, and the Kron flux has been measured for all sources, *psphot* uses these two measurements, along with some additional pixel-level analysis, to determine the size class of the source. Sources identified as extended will be fitted with a galaxy model (or possibly another type of extended source model in special cases). If the source is small compared to a PSF, it is considered to be a *cosmic ray* and masked.

Extended sources are identified as those for which the Kron magnitude is significantly brighter than the PSF magnitude when compared to a PSF star. The value $\delta M_{rmKP} = m_{Kron} - m_{PSF}$, the difference between the PSF and Kron magnitudes, is calculated for each source. The median of δM_{rmKP} is calculated for the PSF stars. This median is subtracted from δM_{rmKP} for each star. The result is divided by the quadrature error of the PSF and Kron magnitudes and called *extNsigma*. If *extNsigma* is larger than *PSPHOT.EXT.NSIGMA.LIMIT* (3.0), the source is considered to be extended and the flag bit *PM_SOURCE_MODE_EXT_LIMIT* is set for the source.

Cosmic rays are identified by a combination of the Kron magnitude and the second-moment width of the source in the minor axis direction. The second-moment in the minor axis direction is calculated from M_{xx}, M_{xy}, M_{yy} as follows:

$$M_{\text{minor}} = \frac{1}{2}(M_{xx} + M_{yy}) - \frac{1}{2}\sqrt{(M_{xx} - M_{yy})^2 + 4M_{xy}^2}$$

If $M_{\text{minor}} < 0.8$ pixels² and the signal-to-noise of the flux measured in the moments analysis > 7 , then the source is identified as a cosmic ray and the associated pixels are masked. These values are tuned empirically for the PV3 analysis based on cosmic rays identified in the GPC1 images. Sources which are determined to be a cosmic ray in this manner have the flag bit *PM_SOURCE_MODE_DEFECT* set.

The pixels of any suspected cosmic ray identified above are examined in additional detail to make a final judgement. The Laplacian edge detection algorithm based on van Dokkum (2001) is used to check for sharp edges in the flux distribution. If the sharpness exceeds a defined limit, then the pixels are masked and the flag bit *PM_SOURCE_MODE_CR_LIMIT* is set for the source.

4.6.6. Full PSF Model Fitting

Once a PSF model has been selected for an image, *psphot* attempts to fit all of the detected sources, with signal-to-noise ratio greater than a user-defined limit, with the PSF model. In the PV3 analysis of the 3π survey data, this limit was set to a signal-to-noise ratio of 20.0 for all analysis stages. In these fits, the dependent parameters are fixed by the PSF model and only the 4 independent source model parameters are allowed to vary in the fit. *psphot* again uses Levenberg-Marquardt minimization for the non-linear fitting. The sources are fitted in their S/N order, starting with the brightest and working down to the user-specified limit, with the other sources subtracted as discussed above. All sources for which a non-linear PSF model has been attempted have the flag bit *PM_SOURCE_MODE_FITTED* set, regardless of the quality of that fit.

Since the PSF model describes the variation of the PSF across the image, the parameters used to fit a specific object are drawn from the model at the position corresponding to the object centroid. Occasionally, a PSF model for an image may not be well determined in all regions of the image. For example, not enough bright stars were available across the full range of the image to model the PSF and the resulting fitted parameters yield non-sensical solutions in areas where detected (fainter) sources are found. In such cases, the PSF fitting is skipped and the flag bit *PM_SOURCE_MODE_BADPSF* is set.

For the PSF model fitting, only pixels within a circular aperture scaled based on the seeing are used. The radius of the circular aperture is set to be a fixed multiple (*PSF_FIT_RADIUS_SCALE*) of σ_w , the width of the Gaussian window function determined based on the analysis of the second moments (see Section 4.4.3). For the PV3 3π analysis, the PSF fit window radius is $7 \times \sigma_w$.

Sources which are blended with other sources may be fitted together as a set of PSFs. Blended objects are identified by first searching for objects for which the PSF fit windows overlap. For a group of such neighboring objects, a contour is determined in the flux image at 25% of the peak of the brightest source in the group. All objects lying within this contour are treated as blends of this brightest source. If other objects in this group exist, the brightest object not already assigned to a blend is used to define the contour for blends of this next object. All objects in the image are tested as possible blends. A single multi-source fit is performed on each group of blended peaks. Sources which are identified as members of a blended group have the flag bit *PM_SOURCE_MODE_BLEND* set, while those for which a blended PSF fit succeeds have the flag bit *PM_SOURCE_MODE_BLEND_FIT* set. *Note that for DR1 & DR2, this option was not used because it tended to prevent galaxies from being fitted as extended objects; the rules for identifying blended stars and galaxies will be revisited in future re-analyses.*

After the PSF model is fitted to each object, *psphot* makes an assessment of the quality of the PSF fits. First, it checks that the non-linear fitting process has converged with a valid fit. The fit for an object can fail if there are too few valid pixels, due to masking or proximity to an edge, or if the parameters are driven to extreme values which are not permitted. In addition, it is possible for the peak finding algorithm to identify peaks in locations which are not actually a normal peak. Some of these cases are in the edges of saturated, bleeding columns from bright stars, in the nearly flat halos of very bright stars, and so on. In these cases, a local peak exists, with a lower nearby sky region. However, the fitted PSF model cannot converge on the peak because it is very poorly defined (perhaps only existing in the smoothed image). In these cases, *psphot* flags the object with the bad bit `PM_SOURCE_MODE_FAIL`. It is also possible in this type of case for the fit to result in a very low or negative value for the flux normalization parameter. Source for which the peak is less than 0.02 are also marked as failing the non-linear PSF fit (`PM_SOURCE_MODE_FAIL`).

Poor fits are also identified by the signal-to-noise and the χ^2 value of the resulting fit. If a source has a PSF S/N ratio lower than a user-defined cutoff (set to 2.0 for the PV3 analysis of the 3π survey), the non-linear PSF fit will be rejected. If the Chi-Square per degree of freedom is greater than a user-defined limit (set to 50.0 for the PV3 analysis of the 3π survey), the non-linear PSF fit will be rejected. These sources are marked with the flag bit (`PM_SOURCE_MODE_POOR`).

Sources which pass the above tests are marked as having a valid non-linear PSF model fit with the flag bit `PM_SOURCE_MODE_NONLINEAR_FIT`. Among these sources, those for which the peak flux is greater than the saturation limit (see Section 4.3) are marked as saturated stars (`PM_SOURCE_MODE_SATSTAR`). These model fits should be considered with caution, but the fluxes and positions may have some validity.

As the sources are fitted to the PSF model, those which survive the exclusion stage are subtracted from the image. The subtraction process modifies the image pixels (removing the fitted flux, though not the locally fitted background) but does not modify the mask or the variance images. The signal-to-noise ratio in the image after subtraction represents the significance of the remaining flux. If the subtractions are sufficiently accurate models of the PSF flux distribution, the remaining flux should be below 1σ significance. In practice the cores of bright stars are poorly represented and may have larger residual significance.

For sources in groups of blended stars, the resulting fits are evaluated independently. Any which are determined to be valid PSF fits are subtracted from the image and kept for future analysis.

4.6.7. Double and Extended Sources

Sources which are judged to be non-PSF-like are confronted with two possible alternative choices. First, the source is fitted with a double-source model. In this pass, the assumption is made that there are two neighboring sources, but the peaks are not resolved. The initial guess for the two peaks is made by splitting the flux of the single source in half and locating the two starting peaks at ± 2 pixels from the original peak along the direction of

the semi-major axis of the sources, as measured from the second moments. In order for the two-source model to be accepted, both sources must be judged as a valid PSF source. Otherwise, the double-PSF model is rejected and the source is fitted with the available non-PSF model or models. Sources for which a double-PSF model is fitted have the flag bit `PM_SOURCE_MODE_PAIR` set.

4.6.8. Non-PSF Sources

Once every source (above the S/N cutoff) has been confronted with the PSF model, the sources which are thought to be extended (resolved) can now be fit with an appropriate model (e.g., galaxy profile or other likely extended shapes). Again, the fitting stage starts with the brightest sources (as judged by the rough S/N measured from the moments aperture) and working to a user defined S/N limit.

psphot will use the user-selected extended source model to attempt these fits. In the configuration system, the keyword `EXT_MODEL` is set to the model of interest. All suspected extended sources are fitted with the model, allowing all of the parameters to float. The initial parameter guesses are critical here to achieving convergence on the model fits in a reasonable time. The moments and the pixel flux distribution are used to make the initial parameter guess. Many of the source parameters can be accurately guessed from the first and second moments. The power-law slope can be guessed by measuring the isophotal level at two elliptical radii and comparing the ratio to that expected.

For each type of extended source model (in fact for all source models), a function is defined which examines the fit results and determines if the fit can be considered as a success or a failure. The exact criteria for this decision depends on the details of the model, and so this level of abstraction is needed. For example, in some case, the range of valid values for each of the parameters must be considered in the fit assessment. In other cases, we may choose to use only the parameter errors and the fit Chi-Square value.

All extended source model fits which are successful are then subtracted from the image as is done for the successful PSF model fits. The background flux is retained, with the result that only the source is subtracted from the image. At this stage, the variance image is not modified.

For the single exposure (CAMERA) and STACK image analysis, these galaxy model fits are only used internally to generate a clean object-subtracted residual image. For the PV3 analysis of the 3π survey, these model fits were saved in the output catalog files, but not loaded to the public database. The `QGAUSS` extended source model was used for the PV3 analysis (see Section 4.5.1). The convolved galaxy model fits (see Section 4.8.3) and the forced galaxy model fits (see Section 5.1) provide more reliable and physically-motivated galaxy models.

For the difference image analysis, a trailed object model is used for the extended sources; these model fit parameters are passed to the Moving Object Processing System (MOPS Denneau et al. 2013).

Any source which is fitted with the extended source model has the flag field `PM_SOURCE_MODE_EXTMODEL` set.

4.7. Faint Source Analysis

After a first pass through the image, in which the brighter sources above a high threshold level have been detected, measured, and subtracted, *psphot* optionally begins a second pass at the image. In this stage, the new peaks are detected on the image with the bright sources subtracted. In this pass, the peak detection process uses the variance image to test the validity of the individual peaks. All peaks with a significance greater than a user-defined minimum threshold are accepted as sources of potential interest.

The sources which are measured in this faint-source stage are clearly low significance detections. The PV3 threshold for the bright source analysis is a signal-to-noise of 20. The flag bit `PM_SOURCE_MODE2_PASS1_SRC` is raised for sources detected in this initial analysis stage. The lower limit cutoff for the faint source analysis in PV3 is a signal-to-noise of 5.0. Sources detected in the faint source stage are fitted with the PSF model using the linear, ensemble fitting process.

In the *psphotStack* version of the code, the 5 filter images are processed together. In this case, any source which is detected in at least two of the five filters are then also measured on the other filter images in which it was not detected above the signal-to-noise limit. The position in the other stack images is fixed based on the pixel coordinates in the images in which the source was detected. Detection in two filters is required in order to avoid excessive forced photometry of spurious detections. There is an interesting class of astronomical objects which are extremely red (e.g., brown dwarfs and high-redshift quasars). Such sources are expected to be detected only in the reddest filter (y_{P1}). For the 3π PV3 processing, we therefore also force the photometry in all filters for sources which are only detected in y_{P1} . All sources which are forced on one image based on detections in other images have the flag bit `PM_SOURCE_MODE2_MATCHED` set.

4.8. Extended Source Analysis

After the initial, fast analysis of the image relying primarily on the PSF model, a complete analysis of the extended source properties may be performed. For PS1 processing, this step is skipped in the nightly (PV0) analysis of individual exposures and only performed for the stacks in the major reprocessings.

The extended source analysis consists of the following types of measurements: 1) an analysis of the radial profile of the surface brightness of the source; 2) measurement of the Petrosian radius and magnitude; 3) convolved galaxy model fits; and 4) photometry in several fixed-sized apertures, both raw and convolved to a defined PSF size.

The extended source analysis is not applied to all object which may be galaxies. Several restrictions are possible within the software. For example, it is possible to limit which objects are processed by their apparent magnitudes, by their signal-to-noise, by an indication if they are in fact extended, by the local stellar density, or by the galactic latitude. Some of these selections may be defined differently for the galaxy model fits and the Petrosian parameters.

For the 3π PV3 processing, both an apparent magnitude cut and a Galactic latitude cut were applied. The apparent magnitude limits for the galaxy model fits are applied to the measured Kron magnitude and depend

on the filter as follows: $(g_{P1}, r_{P1}, i_{P1}, z_{P1}, y_{P1}) = (21.5, 21.5, 21.5, 20.5, 19.5)$. These values were chosen to have roughly similar signal-to-noise in a typical stack image for neutral color objects. The magnitude limits for the Petrosian parameters were set to 25.0 for all filters, far below the detection limits and effectively not limiting the analysis based on apparent magnitude. For both galaxy model fits and Petrosian parameters, the Galactic latitude cut

was defined by $|b| > b_{\min}$ where $b_{\min} = b_0 + r_b e^{\frac{-l^2}{2\sigma_b^2}}$. For the PV3 analysis, $b_0 = 20^\circ$, $r_b = 15^\circ$, $\sigma_b = 50^\circ$. This contour avoids the denser portions of the Galactic plane and bulge, limiting the total time spent on the galaxy modeling analysis at the expense of galaxy photometry in the plane (though Kron photometry is available for those sources).

4.8.1. Radial Profiles

Galaxies with regular profiles, such as elliptical galaxies and regular spiral galaxies, may be described as primarily a radial surface brightness profile, with additional structure acting as a perturbation on that profile. For many galaxies, the azimuthal shape at a given isophotal level may be described as an elliptical contour. To first order, a galaxy may be well described with a single elliptical contour and radial profile.

In order to facilitate the Petrosian photometry analysis below, *psphot* generates a radial profile for each suspected galaxy. This analysis starts by generating a radial profile in 24 azimuthal segments. Near the center of the galaxy, the profile is defined for radial coordinates in steps of 1 pixel, with the closest pixel values interpolated to that radial position. Further from the center, profile is defined using the median of the pixels landing in an annular segment of size $\delta R = r \sin \theta$, rounded up to the nearest integer pixel value. The median of all pixels within a rectangular approximation to the radial wedge is used.

The resulting 24 radial profiles are subject to contamination from neighboring sources or to NAN values from masked pixels. To clean the profiles, pairs of radial profiles from opposite sides of the source are compared. Any masked values are replaced by the corresponding value in the other profile. The minimum of both profiles is then kept for both profiles. The result of this analysis is a set of profiles of the form $f_i(r_i)$. In this case, f_i is effectively the surface brightness for each radius in instrumental counts per pixel. If fewer than 4 radial surface-brightness values are available for the analysis, the source is skipped and the flag bit `PM_SOURCE_MODE2_ECONTOUR_FEW_PTS` is set. Some apparently extended sources are in fact bright stars with central saturation. These sources show up in this analysis as having many NAN-valued pixels in the central regions. During the radial profile analysis, such sources are flagged with the bit `PM_SOURCE_MODE2_RADBIN_NAN_CENTER` and are skipped from the rest of the analysis.

The surface brightness profiles are then used to define the azimuthal contour at a specific isophotal level. This contour will be used to rescale the radial profiles into a single set of profiles normalized by the elliptical contour. This contour is defined by determining the median radius for profile bins with surface brightness in the range $F_{\min} + 0.1F_{\text{range}}$ to $F_{\min} + 0.5F_{\text{range}}$. The result of this analysis is

a value for the radius as a function of the angle for a well-defined surface brightness regime. We then determine the elliptical shape parameters for this elliptical contour: $R_{\text{major}}, R_{\text{minor}}, \theta$. This ellipse is then used to redefine a single radial profile normalized by the elliptical contour:

$$\rho = \sqrt{\frac{x^2}{S_{xx}^2} + \frac{y^2}{S_{yy}^2} + xyS_{xy}}$$

The surface brightness values are sampled at a number of radial annuli, with the radii defined in the configuration (RADIAL.ANNULAR.BINS.LOWER & RADIAL.ANNULAR.BINS.UPPER). For each source, the resulting surface brightness profile is saved in the output FITS table as a vector (PROF_SB). The flux at each radial position and the fill-factor (fraction of pixels used to the total possible) are also saved as equal-length vectors in the FITS table (PROF_FLUX and PROF_FILL). The values of the radial bins are saved in the output file FITS header (RMIN_NN, RMAX_NN).

4.8.2. Petrosian Radii and Magnitudes

Petrosian (1976) defined an adaptive aperture based on a ratio of surface brightnesses. The motivation is to define an aperture which can be determined for galaxies without significant biases as a function of distance from the observer. Since surface brightness in a resolved source is conserved as a function of distance, using a ratio of surface brightness to define a spatial scale results in a spatial scale which is constant regardless of galaxy distance.

To measure the Petrosian radius and flux, we start by defining a series of radial apertures with power-law spacing: $r_{i+1} = 1.25r_i$. We calculate the surface brightness for the annulus from $r_i - r_{i+1}$ by calculating the median of the values in the range $r_i/\sqrt{1.25}$ to $r_{i+1}\sqrt{1.25}$ and dividing the effective area of the annulus corresponding to $r_i - r_{i+1}$.

For any annulus i spanning the radii r_{min} to $r_{\text{max}} = \beta r_{\text{min}}$, the Petrosian Ratio for that annulus is defined as the ratio of the surface brightness in the annulus to the average surface brightness within r_{max} . The Petrosian Radius is defined to be r_{max} for the annulus for which the Petrosian Ratio = 0.2, i.e., the point on the galaxy radial profile at which the surface brightness is 20% of the average surface brightness at that point. If the profile falls below the Petrosian ratio for the first radial bin, the flag bit PM_SOURCE_MODE2_PETRO_RATIO_ZEROBIN is set to note that the Petrosian radius may be poorly determined.

We determine the Petrosian Radius for the galaxy by quadratic interpolation between the last two of the fixed annuli with Petrosian Ratio > 0.2 and the first annulus with Petrosian Ratio < 0.2. In general, the Petrosian Ratio for a galaxy with a regular morphology (spiral or elliptical) is falling monotonically, so this interpolation is unambiguous. However, irregular galaxy morphologies, noise, and/or significant masking can cause the Petrosian Ratio to have rises as well as drops. We track the Petrosian Ratio until the value is no longer significant ($\sigma_{\text{Ratio}} < 2\text{Ratio}$). If the Petrosian ratio drops below 0.2 for more than one radius, we choose the largest such radius. If the Petrosian ratio does not fall below 0.2 for

any of the measured radii, the annulus for which the ratio falls to the lowest (yet still significant) value. In such a case, the flag bit PM_SOURCE_MODE2_PETRO_INSIG_RATIO is set.

Once the Petrosian Radius has been determined, we can now measure the Petrosian Flux : this is defined to be the total flux within an aperture corresponding to $2 \times$ the Petrosian Radius. Using the Petrosian Flux, we can calculate two other interesting radii: R_{50} and R_{90} , the radii inside which 50% and 90% of the total Petrosian flux is contained. Sources for which the Petrosian parameters are successfully measured have the flag bit PM_SOURCE_MODE_EXTENDED_STATS set. Sources for which the Petrosian parameters were attempted, but for which the radial profile analysis failed have the flag bit PM_SOURCE_MODE2_PETRO_NO_PROFILE set.

4.8.3. Convolved Galaxy Model Fits

In the galaxy model fitting stage, sources which meet certain criteria are fitted with analytical models for galaxies. Three traditional analytical galaxy models are implemented in *psphot* and used in the PV3 analysis:

- Exponential profile : $f = I_0 e^{-\rho}$
- DeVaucouleur profile (de Vaucouleurs 1948): $f = I_0 e^{-\rho^{1/4}}$
- Sérsic (Sérsic 1963) : $f = I_0 e^{-\rho^{1/n}}$

where ρ is a normalized radial term: $\rho = \sqrt{\frac{x^2}{R_{xx}^2} + \frac{y^2}{R_{yy}^2} + xyR_{xy}}$. The terms (R_{xx}, R_{yy}, R_{xy}) describe the elliptical contour and the profile scale in all three models and the coordinates x & y are determined relative to the centroids ($x, y = X_{\text{chip}} - x_0, Y_{\text{chip}} - y_0$). Including the normalization (I_0) and a local sky value, the Exponential and DeVaucouleur profiles have 7 free parameters and the Sérsic profile has the additional free parameter of the Sérsic index n . In this stage, the galaxy model is convolved with an approximation to our best guess for the PSF model at the location of the galaxy.

Sources which passed the extended source restrictions described above were fitted with all three galaxy models, unless (a) the morphological test identified the source as a likely cosmic ray (Section 4.6.5) or (b) the peak of the PSF profile was above the saturation limit for the chip (see the discussion in Waters et al. 2016, regarding the masking of saturated pixels). All sources for which the extended source model fits were attempted the flag bit PM_SOURCE_MODE2_EXT_FITS_RUN set. If any of the attempted model fits failed, then the flag bit PM_SOURCE_MODE2_EXT_FITS_FAIL is set. If all model fits failed, then the flag bit PM_SOURCE_MODE2_EXT_FITS_NONE is set.

Before the non-linear fitting may be performed, it is necessary to determine initial values for the parameters to be fitted. For each of the three model types, the position determined from the PSF fitting analysis is used as the initial centroid x_0, y_0 . A guess for the terms (R_{xx}, R_{yy}, R_{xy}) is generated based on the second moments. The guess does not attempt to use the PSF model to adjust the (R_{xx}, R_{yy}, R_{xy}) values; it was found that such a guess tended to be too small and resulted in more

iterations rather than fewer. The 1st radial moment (see 4.4.3) is used to estimate the effective radius of the model based on the results of Graham & Driver (2005, Table 1). They quantify the relationships between the first radial moment used to calculate a Kron Magnitude and the effective radius for different Sérsic index values, n . Since the Exponential and DeVaucouleur models are equivalent to Sérsic models with $n = 1$ and 4 , respectively, this work can be used to generate the initial effective radius values for all 3 model types. Once the effective radius is chosen, the second moments are used to define the aspect ratio and position angle of the elliptical contour. The Kron flux is used to generate a guess for the normalization, applying an appropriate scale factor based on the (R_{xx}, R_{yy}, R_{xy}) values, generated by integrating normalized Sérsic models and determining the relationship between the central intensity and the integrated flux as a function of the Sérsic index.

The PSF-convolved galaxy model fitting analysis uses the Levenberg-Marquardt minimization method to determine the best fit. In this process, the χ^2 value to be minimized is:

$$\chi^2(\bar{a}) = \sum_p \frac{1}{\sigma_p^2} [I_p - M_p(\bar{a}) \otimes \text{PSF}]^2$$

where I_p represents the pixel values in the image (within some aperture) and $M_p(\bar{a})$ represents the unconvolved galaxy model, a function of a number of parameters \bar{a} , which is then convolved with the PSF model.

We simplify this by defining:

$$f_p(a_m) = \frac{1}{\sigma_p} (I_p - M_p \otimes \text{PSF}) \quad (27)$$

$$(28)$$

To determine the minimization, we need the gradient and laplacian of χ^2 with respect to the model parameters, a_m :

$$\chi^2(\bar{a}) = \sum_p f_p^2 \quad (29)$$

$$2\nabla\chi^2 = \sum_p f_p \frac{\partial f_p}{\partial a_m} \quad (30)$$

$$\nabla^2\chi^2 \sim H_{m,n} \quad (31)$$

$$2H_{m,n} = \sum_p \frac{\partial f_p}{\partial a_m} \frac{\partial f_p}{\partial a_n} \quad (32)$$

where we have approximated the Laplacian with the Hessian matrix, $H_{m,n}$ by dropping the second-derivatives (which are assumed to be a small perturbation). Since

$$\frac{\partial f_p}{\partial a_m} = -\frac{1}{\sigma_p} \frac{\partial M_p \otimes \text{PSF}}{\partial a_m}$$

and since the order of the derivative and convolution may be exchanged, we can write these in terms of the convolved image of the model and the convolved images of the derivatives of the model M_p with respect to the model parameters, a_m :

$$\mathcal{M}_p = M_p \otimes \text{PSF} \quad (33)$$

$$\mathcal{M}'_{p,m} = \frac{\partial M_p}{\partial a_m} \otimes \text{PSF} \quad (34)$$

$$2\nabla\chi^2 = -\sum_p \frac{I_p - \mathcal{M}_p}{\sigma_p} \mathcal{M}'_{p,m} \quad (35)$$

$$2H_{m,n} = \sum_p \frac{1}{\sigma_p^2} \mathcal{M}'_{p,m} \mathcal{M}'_{p,n} \quad (36)$$

The gradient vector and Hessian matrix are used in the Levenberg-Marquardt minimization analysis using the standard technique of determining a step from the current set of model parameters to a new set by solving the matrix equation:

$$(1 + \lambda_{m,n})H_{m,n} = \delta\nabla\chi^2$$

where $\lambda_{m,n}$ is zero for $m \neq n$ and for $m = n$ set to be large when the last iteration produced a large change in the parameters compared to the local-linear expectation and small when the last change was small. The iteration ends when the change in the parameters is small and/or the change in the χ^2 value is small.

In the analysis, convolved galaxy fit, the galaxy model image and the model derivative images must be convolved with the PSF at each iteration step. To save computation time, this convolution is performed using a circularly symmetric approximation of the PSF model, with the PSF model scale size set to the average of the major and minor axis direction scale size of the full PSF model, with the same radial profile term as the PSF model. The convolution is performed directly using the circular symmetry to reduce the number of multiplications performed: all points in the 2D circularly symmetric PSF model which have the same radial pixel coordinate can be evaluated in the convolution by summing up the corresponding pixels in the (galaxy model) image to be convolved before multiplying by the PSF model profile at that radial coordinate. This approximation reduces the number of multiplications by a factor of ~ 8 for larger radii. For the small size of the PSF model used to convolve the galaxy model images, it was found that this direct convolution was faster than using an FFT-based convolution.

For the Exponential and DeVaucouleur fits, all parameters are fitted in the non-linear minimization stage. For the Sérsic model, we do not fit the index within the Levenberg-Marquardt analysis. Instead, we start with a coarse grid search over a range of possible index values, ($n = 0.5, 1.0, 1.5, 2.0, 3.0, 4.0, 5.0, 6.0$) and a range of possible values for R_{eff} based on the value of R_1 , the first radial moment. For a given value of the Sérsic index, the R_{eff} is related to the 1st radial moment by the scale factor specified by Graham & Driver. We use the observed value of the 1st radial moment and try R_{eff} values of a factor of (0.8, 0.9, 1.0, 1.12, 1.25) times the value predicted by the Graham and Driver equation. For each of these steps, the aspect ratio and position angle are held constant and the normalization is determined to minimize the χ^2 .

We next perform 3 Levenberg-Marquardt minimization fits allowing the shape parameters (R_{xx}, R_{yy}, R_{xy}) and the normalization to be fitted, holding the centroid (x_0, y_0) , Sérsic index n , and sky constant. In these fits, the index n is set to the minimum value previously calculated as well as values halfway to the next, and previous, values in the grid above. E.g., if the minimum fitted index value is 3.0, then the LMM fits are performed us-

ing $n = 2.5, 3.0, 3.5$. The resulting χ^2 values are then used to perform quadratic interpolation to find the index n which produces the locally minimum χ^2 value. Finally, this best-fit index value is held constant while Levenberg-Marquardt minimization is used to find the best fit values of all other parameters. Sources for which a convolved galaxy model fit was successful have the flag bit `PM_SOURCE_MODE_EXTENDED_FIT` set.

The central pixel of the Sérsic, DeVaucouleur, and Exponential models requires special handling. When comparing an analytical model to the pixelized image recorded by a CCD, one normally treats the value in a pixel as equivalent to the value of the model at the center of the pixel. However, in reality, the number of counts observed in a pixel represents the integral of the surface brightness across the area of the pixel. This average will be equal to the central surface brightness times the area of a pixel as long as the second and higher derivatives of the analytical model are zero. However, if the first and second derivatives are non-zero, the curvature of the function within the pixel will make the integral differ from the central surface brightness times a fixed pixel area. If the curvature of the model function is sufficiently large, this difference will have a significant impact on the evaluation of the model. This situation is particularly true for the central portion of the Sérsic-like model functions.

In order to accurately compare the observed galaxy flux distribution to a model, it is necessary to integrate the pixel flux for a given set of model parameter values. This could be done in a numerical fashion, but in practice brute-force evaluation of the numerical integral is computationally very expensive, requiring many evaluations of the model function. Within *psphot*, we bypass this problem by defining a set of pre-calculated images for the central 9 pixels (the 3×3 grid of pixels centered on the peak). These pixel images are defined at higher resolution, with 11 subpixels per real CCD pixel. The pre-calculated images are generated for a series of values for the following parameters: Sérsic index, effective radius, axial ratio. We then select the closest image to our specific case, and integrate over the true sub-pixels relevant for our position and model. We have thus turned the problem from thousands of evaluations of the full galaxy model to ~ 100 straight additions, or up to $6 \times$ that number if we interpolate between any of the parameters.

4.8.4. Fixed Aperture Photometry

For some science goals, a well-measured color of a galaxy is more important than an accurate total magnitude. In the case of PS1, the image quality variations for stacks of different filters presents a serious challenge for the determination of precise colors. *psphot* determines a set of PSF-matched radial aperture flux measurements in order to minimize the impact of the stack image quality variations.

In *psphotStack*, the stack analysis version of *psphot*, the 5 filter images are processed together. After the PSF models have been fitted and a best set of galaxy models have been determined, three sets of fixed circular apertures are measured. In the first set, the fluxes in the apertures are measured using the raw stack images. The centers of the apertures for each source across the 5 filters are fixed so that the pixels represent the equivalent

portions of the same galaxy for all 5 filters. In this analysis, the best model for each source is subtracted from the image pixels for all sources excluding the source in consideration. The 'best model' is determined based on the minimum χ^2 value for the model fits.

In addition to the raw fixed circular apertures, the stack images are each convolved with a circular Gaussian with σ chosen to yield an image with a typical FWHM of 6 pixels ($1.5''$). The full set of circular apertures are again measured on these convolved images. Again, the best source models are subtracted from the image for sources not being measured. This subtraction includes the convolution to smooth the model to the effective FWHM of the convolved image. The entire procedure is then repeated with a target FWHM of 8 pixels ($2''$).

For the PV3 analysis of the 3π survey data, the fluxes are measured for a set of up to 9 circular apertures with sizes chosen to match the similar circular apertures measured by the SDSS analysis. These apertures have radii of (4.16, 7.04, 12.0, 18.56, 29.76, 45.68, 72.80, 112.80, 176.88) pixels = (1.04, 1.76, 3.00, 4.64, 7.44, 11.42, 18.20, 28.20, 44.22) arcseconds. If the object is too faint, the larger apertures will be largely noise and the computation is wasteful. We only calculate the circular apertures out to the second aperture larger than the "sky radius" (defined in Section 4.6.3), but we calculate photometry for at least the smallest 4 apertures. Sources for which photometry in these fixed aperture are calculated have the flag bit `PM_SOURCE_MODE_RADIAL_FLUX` set.

4.9. Aperture Correction and Total Aperture Fluxes

A PSF model will always fail to describe the flux of the stellar sources at some level. For high-precision photometry, we need to be able to correct for the difference between the PSF model fluxes and the total flux of the sources. In the end, all astronomical photometry is in some sense a relative measurement between two images. Whether the goal is calibration of a science image taken at one location to a standard star image at another location, or the goal is simply the repetitive photometry of the same star at the same location in the image, it is always necessary to compare the photometry between two images. If this measurement is to be consistent, then the measurement must represent the flux of the stars in the same way regardless of the conditions under which the images were taken, at least within some range of normal image conditions. So, for example, two images with different image quality, or with different tracking and focus errors, will have different PSF models. To the extent the PSF model is inaccurate, the measured flux of the same source in the two images will be different (even assuming all other atmospheric and instrumental effects have been corrected). The amplitude of the error will be determined by how inconsistently the models represent the actual source flux.

Aperture photometry attempts to avoid these problems, but introduces other difficulties. In aperture photometry, if a large enough aperture is chosen, the amount of flux which is lost will be a small fraction of the total source flux. Even more importantly, as the image conditions change, the amount lost will change by an even smaller fraction, at least for a large aperture. This can be seen by the fact that the dominant variations in the image quality are in the focus, tracking and seeing. All of

these errors initially affect the cores of the stellar images, rather than the wide wings. The wide wings are largely dominated by scattering in the optics and scattering in the atmosphere. The amplitude and distribution of these two scattering functions do not change significantly or quickly for a single telescope and site. Aperture photometry can then be used to correct the PSF photometry.

The difficulty for aperture photometry is the need to make an accurate measurement of the local background for each source. As the aperture grows, errors in the measurement of the sky flux start to become dominant. If the aperture is too small, then variations in the image quality are dominant. The brighter is the source, the smaller is the error introduced by the large size of the aperture. However, the number of very bright stars is limited in any image, and of course the brighter stars are more likely to suffer from non-linearity or saturation.

In order to thread the needle between these effects, *psphot* measures the aperture photometry on a modest-sized aperture, and then uses the PSF model to extrapolate to a large aperture. When the PSF fluxes are calculated, the aperture flux for the modest-sized aperture is also determined. The aperture is a circular aperture with radius set to a fixed multiple (`PSF_APERTURE_SCALE`) of σ_w , the width of the Gaussian window function determined based on the analysis of the second moments (see Section 4.4.3). For the PV3 3π analysis, the aperture window radius is $4.5 \times \sigma_w$, while the large reference aperture radius is set to 25 pixels (`PSF_REF_RADIUS` = 6''.4). These corrected aperture magnitudes are saved in the output catalogs as `AP_MAG`, the uncorrected aperture magnitudes are saved as `AP_MAG_RAW`, and the radius used to measure the raw aperture flux is saved as `AP_MAG_RADIUS`. The corresponding flux and the flux error are saved as `AP_FLUX` and `AP_FLUX_SIG`.

With these aperture magnitudes in hand, it is now possible to make an average correction to the PSF magnitudes to bring the PSF and aperture magnitudes to the same system. This correction is measured using the same stars from which the PSF model is measured, as long as the PSF magnitude error for the star is less than 0.03 mag. The correction is calculated using the weighted average of the values $m_{AP} - m_{PSF}$. Since the PSF may vary across the image, the correction is determined as a function of position in the image. Like the PSF model, the 2D variations of the aperture correction may be modeled as a polynomial or via interpolation in a grid. For the 3π PV3 analysis, a grid with a maximum of 6×6 samples per GPC1 chip image was used. The reported PSF magnitudes for all objects have this aperture correction applied.

psphot allows a collection of PSF model functions to be tried on all PSF candidate sources. For each model test, the above corrected ApResid scatter is measured. The PSF model function with the smallest value for the ApResid scatter is then used by *psphot* as the best PSF model for this image. The number of models to be tested is specified by the configuration keyword `PSF_MODEL_N`. The configuration variables `PSF_MODEL_0`, `PSF_MODEL_1`, through `PSF_MODEL_N - 1` specify the names of the models which should be tested.

5. FORCED PHOTOMETRY MODES

Traditionally, projects which use multiple exposures to increase the depth and sensitivity of the observations have generated something equivalent to the stack images produced by the IPP analysis (c.f. CFHT Legacy survey, COSMOS, etc). In theory, the photometry of the stack images produces the “best” photometry catalog, with best sensitivity and the best data quality at all magnitudes. In practice, these images have some significant limitations due to the difficulty of modeling the PSF variations. This difficulty is particularly severe for the Pan-STARRS 3π survey stacks due to the combination of the substantial mask fraction of the individual input exposures, the large intrinsic image quality variations within a single exposure, and the wide range of image quality conditions under which data were obtained and used to generate the 3π PV3 stacks.

For any specific stack, the point spread function at a particular location is the result of the combination of the point spread functions for those individual exposures which went into the stack at that point. Because of the high mask fraction, the exposures which contributed to pixels at one location may be somewhat different just a few tens of pixels away. In the end, the stack images have a effective point spread function which is not just variable, but changing significantly on small scales in a highly textured fashion.

Any measurement which relies on a good knowledge of the PSF at the location of an object needs to determine the PSF variations present in the stack image or the measurement will be somewhat degraded. The highly textured PSF variations make this a very challenging problem: not only would such a PSF model require an unusually fine-grained PSF model, there would likely not be enough PSF stars in a given stack image to determine the model at the resolution required. The IPP photometry analysis code uses a PSF model with 2D variations using a grid of at most 6×6 samples per sky-cell, a number reasonably well-matched to the density of stars at most moderate Galactic latitudes. This scale is far too large to track the fine-grained changes apparent in the stack images.

As a result, PSF photometry as well as convolved galaxy models in the stack are degraded by the PSF variations. Aperture-like measurements are in general not as affected by the PSF variations, as long as the aperture in question is large compared to the FWHM of the PSF.

The IPP analysis solves this problem by starting with the sources detected in the stack images and performing forced photometry on the individual warp images used to generate the stack, and then combining the resulting measurements to determine a high-quality average value. This forced-photometry analysis is performed using the *psphotFullForce* variant of *psphot*.

In this program, the positions of sources are loaded from the output catalog of the stack photometry. Candidates PSF stars are pre-identified as those stars used to generate the PSF model in the stack photometry analysis. A PSF model is generated for each input warp image based on those stars; PSF stars which are excessively masked on a particular image are not used to model the PSF. The PSF model is fitted to all of the known source positions in the warp images. Aperture magnitudes, Kron magnitudes, and moments are also measured at this stage for each warp. Note that the flux measure-

ment for a faint, but significant, source from the stack image may be at a low significance (less than the 5σ criterion used when the photometry is not run in this forced mode) in any individual warp image; the measured flux may even be negative due to statistical fluctuations. When combined together, these low-significance measurements result in a significant measurement as the signal-to-noise increases with the combination of more data.

Individual warp images are processed independently with separate executions of the *psphotFullForce* program. Sources which are loaded by *psphotFullForce* for analysis are marked with the flag bit `PM_SOURCE_MODE_EXTERNAL`. This bit is also used to mark user-supplied sources loaded for analysis by the regular version of *psphot*. Once all of the forced photometry measurements (for point sources as well as galaxies, discussed below) are completed for all of the warps which contributed to a stack image, the measurements are combined together by other portions of the IPP system. The PSF photometry measurements are combined in the context of the DVO database system (Magnier et al. 2017), including recalibration of the zero points for the individual warp.

5.1. Forced Galaxy Models

The convolved galaxy models are also re-measured on the warp images by the *psphotFullForce* analysis. In this analysis, the galaxy models determined from the stack image analysis are used to seed the analysis in the individual warp images. The motivation of this analysis is the same as the forced PSF photometry: the PSF of the stack image is poorly determined due to the masking and PSF variations in the inputs. Without a good PSF model, the PSF-convolved galaxy models are of limited accuracy.

In the forced galaxy model analysis, we assume that the galaxy position and position angle, along with the Sérsic index if appropriate, have been sufficiently well determined in the analysis of the stack image. In this case, the goal is to determine the best values for the major and minor axis of the elliptical contour and at the same time the best normalization corresponding to the best elliptical shape, and thus the best galaxy magnitude value.

For each warp image, the stack values for the major and minor axis are used as the center of a grid search of the major and minor axis parameter values. The grid spacing is defined as a function of the signal-to-noise of the galaxy in the stack image so that bright galaxies are measured with a much finer grid spacing than faint galaxies. For the PV3 3π analysis, a 5×5 grid was used; values in both the major and minor axis directions of $(1 - \frac{3.0}{S/N}, 1 - \frac{1.5}{S/N}, 1.0, 1 + \frac{1.5}{S/N}, 1 + \frac{3.0}{S/N})$ times the dimension are tested. For each grid point, the major and minor axis values at that point are used to generate the model. The model is then convolved with the PSF model for the warp image at that point. The resulting convolved model is then compared to the warp pixel data values and the best fit normalization value is determined. The integrated flux, flux error, and the χ^2 value for each grid point are recorded.

For a given galaxy, the result is a collection of χ^2 val-

ues, fluxes, and flux errors for each of the grid points spanning all warp images. A single χ^2 grid can then be made by combining each grid point across the inputs. The combined χ^2 for a single grid point is simply the sum of all χ^2 values at that point. If, for a single warp image, the galaxy model is excessively masked, then that image will be dropped for all grid points for that galaxy. The reduced χ^2 values can be determined by tracking the total number of pixels used across all inputs to generate the combined χ^2 values. From the combined grid of χ^2 values, the point in the grid with the minimum χ^2 is found. Quadratic interpolation is used to determine the major, minor axis values for the interpolated minimum χ^2 value. The errors on these two parameters is then found by determining the contour at which the χ^2 increases by 1.

In this way, the forced galaxy model analysis uses the PSF information from each warp image to determine a best set of convolved galaxy models for each galaxy model measured for the stack image.

6. DIFFERENCE IMAGE PHOTOMETRY

Among the primary science drivers for Pan-STARRS are the detection of moving objects (e.g., asteroids) and explosive transient sources (e.g., supernovae). For both of these situations, difference images are commonly used to remove the clutter of the static stars and galaxies. In the Pan-STARRS system, difference images are generated using the PSF-matching technique described by (e.g., Alard & Lupton 1998). The description of the Pan-STARRS implementation is given by Price et al. (2017). The analysis of the sources detected in these difference images uses a portion of the *psphot* code embedded in the program, *ppSub*, which generates those image.

The analysis of the difference image follows the same basic steps as other *psphot* versions with some minor modifications (see Table 1), as follows. The background subtraction is performed before the PSF matching and image subtraction is performed. The PSF model construction stage is not possible in the difference image due to the lack of valid sources. Instead, the PSF model from is generated from the positive image, after PSF-matching but before the subtraction is performed. Because we do not expect to have a large number of sources, only a single source detection pass is performed, and at the lowest signal-to-noise threshold. Only linear PSF model fitting is performed using the centroid determined from the analysis of the source moments.

For the difference images, the galaxy model analysis is not relevant. In a properly-constructed difference image, galaxies are unlikely to remain behind as significant sources. Most real sources in the difference image will be PSF-like and will consist of photometrically variable sources (flare stars, supernovae, etc) or astrometrically variable sources (high-proper motion stars or solar-system bodies). There are three likely classes of sources which will not be well represented by the PSF model, as discussed below.

Fast-moving solar-system objects will appear as short streaks. For example, a fast solar system object may have an apparent rate of 0.5 degrees per hour, translating to 15 arcseconds in a 30 second exposure. Even a main belt asteroid at roughly 1 AU has reflex motion of approximately 1 degree per day, equivalent to 1.25 arcsec in a

30 second exposure, and may be noticeably smeared and non-PSF-like. In *psphot*, we use a trailed-star model to characterize these types of sources. This model is fitted in the same portion of the code which performs the unconvolved galaxy model analysis.

In some cases, the stars in the two images may be somewhat offset. For specific stars, this offset may be due to differential chromatic aberration from the atmosphere or the optics, or from modest proper motion. If the astrometric solution for one of the two images is insufficiently accurate, all stars in large portions of the images may be noticeably displaced. In both of these situations, the stars will appear as PSF dipoles in the difference images. The positive and the negative images will have stellar profiles, but they will be offset and will not subtract well. The two components may not have the same amplitude. In theory, a PSF-dipole model could be used to fit these types of sources, with free parameters of the two centroids and the two fluxes. In practice in *psphot*, we use a number of non-parametric pixel-level statistics in an attempt to detect these cases.

For the difference images, we measure the following quantities for each of the detections, using only pixels within the photometry aperture. First, we count the number of masked pixels (*nMask*), the number of pixels with positive flux (*nGood*), and the number of pixels with negative flux (*nBad*). We also add the total flux in positive pixels (*fGood*) and total absolute value of the flux in negative pixels (*fBad*). Using these values, We report the following quantities:

- *nGood*
- $fRatio = fGood / (fGood + fBad)$
- $nRatioBad = nGood / (nGood + nBad)$
- $nRatioMask = nGood / (nGood + nMask)$
- $nRatioAll = nGood / (nGood + nMask + nBad)$

We also attempt to place the difference image detections in the context of the input images, both the positive (subtrahend) and negative (minuend) images. We identify the closest source in both the positive and negative images to the detection in the difference image, out to a maximum of `INPUT.MATCH.RADIUS` (= 50 pixels), but only if the source in those images has a signal-to-noise greater than `INPUT.MATCH.MIN.SN` (= 10). If there is a close neighbor in the positive image, and the difference in the magnitudes of the source in that image and the source in the difference image is less than 5σ , then the bit `PM_SOURCE_MODE2_DIFF_SELF_MATCH` = 0x00000800 is raised in `mask2` as these two detections are likely the same flux (i.e., detection of an isolated source).

If the difference image detection is matched to a nearby source in the positive image, then the signal-to-noise of the neighbor is saved as `DIFF_SN_P` and the distance in pixels between the difference detection and positive detection is saved as `DIFF_R_P`. Similarly, for a neighbor in the negative image, these values are saved as `DIFF_SN_M` and `DIFF_R_M`. Additional `mask2` bits are also raised: if the difference detection is only associated with one of the two input images,

then the bit `PM_SOURCE_MODE2_DIFF_WITH_SINGLE` = 0x00000001 is raised, while a difference detection which has a match in both input images has `PM_SOURCE_MODE2_DIFF_WITH_DOUBLE` = 0x00000002 raised.

Comets appear in the difference images as a non-PSF sources. Their 2-D structure includes both the flux from the coma (with a typical power-law profile) and flux from the tail (with a more complex flux distribution). We use the Kron magnitudes to identify possibly extended objects which may be cometary in nature.

For a difference image, both positive and negative sources will be present. The basic peak detection algorithm will only trigger for the positive sources. In the *ppSub* program, both the $A - B$ and the $B - A$ images are sent to the *psphot* routine for source detection and characterization.

Note that the variance image for a difference image must be generated from the two positive images used to construct the difference. It is possible to run *psphot* as an external program on a difference image generated previously. In this case, the variance image and the PSF model must be supplied as well as the difference image.

The Pan-STARRS1 Surveys (PS1) have been made possible through contributions of the Institute for Astronomy, the University of Hawaii, the Pan-STARRS Project Office, the Max-Planck Society and its participating institutes, the Max Planck Institute for Astronomy, Heidelberg and the Max Planck Institute for Extraterrestrial Physics, Garching, The Johns Hopkins University, Durham University, the University of Edinburgh, Queen's University Belfast, the Harvard-Smithsonian Center for Astrophysics, the Las Cumbres Observatory Global Telescope Network Incorporated, the National Central University of Taiwan, the Space Telescope Science Institute, the National Aeronautics and Space Administration under Grant No. NNX08AR22G issued through the Planetary Science Division of the NASA Science Mission Directorate, the National Science Foundation under Grant No. AST-1238877, the University of Maryland, and Eotvos Lorand University (ELTE) and the Los Alamos National Laboratory.

REFERENCES

- Alard, C. & Lupton, R. H. 1998, *ApJ*, 503, 325
 Antilogus, P., Astier, P., Doherty, P., Guyonnet, A., & Regnault, N. 2014, *Journal of Instrumentation*, 9, C03048
 Bertin, E. & Arnouts, S. 1996, *A&AS*, 117, 393
 Buonanno, R., Buscema, G., Corsi, C. E., Ferraro, L., & Iannicola, G. 1983, *A&A*, 126, 278
 Chambers, K. C., Magnier, E. A., Metcalfe, N., & et al. 2017, *ArXiv e-prints*
 de Vaucouleurs, G. 1948, *Annales d'Astrophysique*, 11, 247
 Denneau, L., Jedicke, R., Grav, T., Granvik, M., Kubica, J., Milani, A., Vereš, P., Wainscoat, R., Chang, D., Pierfederici, F., Kaiser, N., Chambers, K. C., Heasley, J. N., Magnier, E. A., Price, P. A., Myers, J., Kleyna, J., Hsieh, H., Farnocchia, D., Waters, C., Sweeney, W. H., Green, D., Bolin, B., Burgett, W. S., Morgan, J. S., Tonry, J. L., Hodapp, K. W., Chastel, S., Chesley, S., Fitzsimmons, A., Holman, M., Spahr, T., Tholen, D., Williams, G. V., Abe, S., Armstrong, J. D., Bressi, T. H., Holmes, R., Lister, T., McMillan, R. S., Micheli, M., Ryan, E. V., Ryan, W. H., & Scotti, J. V. 2013, *PASP*, 125, 357

- Flewelling, H. A., Magnier, E. A., Chambers, K. C., Heasley, J. N., Holmberg, C., Huber, M. E., Sweeney, W., Waters, C. Z., Chen, T., Farrow, D., Hasinger, G., Henderson, R., Long, K. S., Metcalfe, N., Nieto-Santisteban, M. A., Norberg, P., Saglia, R. P., Szalay, A., Rest, A., Thakar, A. R., Tonry, J. L., Valenti, J., Werner, S., White, R., Denneau, L., Draper, P. W., Jedicke, R., Kudritzki, R.-P., Price, P. A., Chastel, S., McClean, B., Postman, M., & Shiao, B. 2016, ArXiv e-prints
- Gruen, D., Bernstein, G. M., Jarvis, M., Rowe, B., Vikram, V., Plazas, A. A., & Seitz, S. 2015, *Journal of Instrumentation*, 10, C05032
- Hodapp, K. W., Siegmund, W. A., Kaiser, N., Chambers, K. C., Laux, U., Morgan, J., & Mannery, E. 2004, in *Proc. SPIE*, Vol. 5489, *Ground-based Telescopes*, ed. J. M. Oschmann, Jr., 667–678
- Huber, M., TBD, A., TBD, B., & et al. 2017, ArXiv e-prints
- Kron, R. G. 1980, *ApJS*, 43, 305
- Lupton, R., Gunn, J. E., Ivezić, Z., Knapp, G. R., & Kent, S. 2001, in *Astronomical Society of the Pacific Conference Series*, Vol. 238, *Astronomical Data Analysis Software and Systems X*, ed. F. R. Harnden, Jr., F. A. Primiini, & H. E. Payne, 269
- Madsen, K., Nielsen, H. B., & Tingleff, O. 2004, *Methods for Non-Linear Least Squares Problems* (Lyngby: Informatics and Mathematical Modelling Technical University of Denmark)
- Magnier, E. A., Schlafly, E. F., Finkbeiner, D. P., & et al. 2017, ArXiv e-prints
- Magnier, E. A., Schlafly, E. F., Finkbeiner, D. P., Tonry, J. L., Goldman, B., Röser, S., Schilbach, E., Chambers, K. C., Flewelling, H. A., Huber, M. E., Price, P. A., Sweeney, W. E., Waters, C. Z., Denneau, L., Draper, P., Hodapp, K. W., Jedicke, R., Kudritzki, R.-P., Metcalfe, N., Stubbs, C. W., & Wainscoat, R. J. 2016, ArXiv e-prints
- Moffat, A. F. J. 1969, *A&A*, 3, 455
- Onaka, P., Tonry, J. L., Isani, S., Lee, A., Uyeshiro, R., Rae, C., Robertson, L., & Ching, G. 2008, in *Proc. SPIE*, Vol. 7014, *Ground-based and Airborne Instrumentation for Astronomy II*, 70140D
- Peng, C. Y., Ho, L. C., Impey, C. D., & Rix, H.-W. 2002, *AJ*, 124, 266
- Petrosian, V. 1976, *ApJ*, 209, L1
- Press, W. H., Teukolsky, S. A., Vetterling, W. T., & Flannery, B. P. 1992, *Numerical recipes in C. The art of scientific computing* (Cambridge: University Press, 1992, 2nd ed.)
- Price, P. A., TBD, A., TBD, B., & et al. 2017, ArXiv e-prints
- Schechter, P. L., Mateo, M., & Saha, A. 1993, *PASP*, 105, 1342
- Sérsic, J. L. 1963, *Boletín de la Asociacion Argentina de Astronomia La Plata Argentina*, 6, 41
- Stetson, P. B. 1987, *PASP*, 99, 191
- Tonry, J. & Onaka, P. 2009, in *Advanced Maui Optical and Space Surveillance Technologies Conference*, E40
- Tonry, J. L., Stubbs, C. W., Lykke, K. R., Doherty, P., Shivvers, I. S., Burgett, W. S., Chambers, K. C., Hodapp, K. W., Kaiser, N., Kudritzki, R.-P., Magnier, E. A., Morgan, J. S., Price, P. A., & Wainscoat, R. J. 2012, *ApJ*, 750, 99
- van Dokkum, P. G. 2001, *PASP*, 113, 1420
- Waters, C. Z., Magnier, E. A., Price, P. A., Chambers, K. C., Draper, P., Flewelling, H. A., Hodapp, K. W., Huber, M. E., Jedicke, R., Kaiser, N., Kudritzki, R.-P., Lupton, R. H., Metcalfe, N., Rest, A., Sweeney, W. E., Tonry, J. L., Wainscoat, R. J., Wood-Vasey, W. M., & Builders, P. 2016, ArXiv e-prints